Northeastern Pacific oxygen minimum zone variability over the past 70 kyr: Impact of biological production and oceanic ventilation

Olivier Cartapanis, K. Tachikawa, Edouard Bard

Northeastern Pacific oxygen minimum zone variability over the past 70 kyr: Impact of biological production and oceanic ventilation

Olivier Cartapanis,[1] Kazuyo Tachikawa,[1] and Edouard Bard[1]

Received 27 January 2011; revised 28 July 2011; accepted 31 July 2011; published 29 October 2011.

[1] During the last glacial period, the Oxygen Minimum Zone (OMZ) within the northeastern Pacific Ocean strengthened and weakened on a millennial time scale, demonstrating a tight linkage with northern high latitude climate, although the precise mechanisms responsible remain unknown. Core MD02–2508, retrieved off Baja California, was analyzed for major and trace elements (Br, Ca, Ti, Fe, Mn, and Sr) using a XRF scanner and redox-sensitive trace elements (Cu, Ni, Cd, As, V, Cr, Mo, and U) using the ICP-MS. The trace element content, the Fe/Ti ratio, and Br-based organic carbon exhibit higher values during the Holocene and during warm Dansgaard-Oeschger events than during the Last Glacial Maximum (LGM), stadials, and Heinrich (H) events. A principal component analysis of the element/Al ratio indicated that the following two main factors controlled the chemical composition of the sediments: (1) export production, as represented by organic carbon, that was lower during cold periods; and (2) regional intermediate water oxygenation, as represented by U and Mo variability, that was not supported by a change in export production. The latter suggests that intermediate water oxygenation improved during H events, but slightly deteriorated during late Marine Isotope Stage (MIS) 3 and MIS 2. A local biogeochemical effect, forced by atmospheric processes, impacted the LGM and H events in the same manner. Whereas regional intermediate oceanic circulation varied in an opposite manner during the LGM and H events, possibly as a result of the global reorganization of intermediate water circulation during the LGM.

Citation: Cartapanis, O., K. Tachikawa, and E. Bard (2011), Northeastern Pacific oxygen minimum zone variability over the past 70 kyr: Impact of biological production and oceanic ventilation, *Paleoceanography*, *26*, PA4208, doi:10.1029/2011PA002126.

1. Introduction

[2] Records of the oxygen isotope composition in Greenland ice cores show seesaw-like air temperature variations at the millennial-scale over the last glacial period that are often referred to as Dansgaard-Oeschger events (DO) [*Dansgaard et al.*, 1993; *Johnsen et al.*, 2001]. A few cold DO events in Greenland were associated with an ice rafted debris layer in the North Atlantic Ocean and are referred to as Heinrich events (H), that corresponded to large continental ice discharges into the ocean [*Heinrich*, 1988; *Broecker et al.*, 1992]. Anomalously fresh water inputs into the North Atlantic Ocean are thought to have impacted North Atlantic Deep Water (NADW) formation and to have reduced poleward heat transport, leading to a large temperature decrease over the North Atlantic Ocean [*Clement and Peterson*, 2008, and references therein]. H-DO scale climate variability is thought to have extended to lower latitudes into Oxygen Minimum Zones (OMZ) within the northeastern Pacific Ocean and the Arabian Sea [*Schulz et al.*, 1998; *Schulte et al.*, 1999; *Altabet et al.*, 2002; *Ortiz et al.*, 2004]. Proxy records and modeling studies suggest that the OMZ intensified during interstadials (warm DO events), and weakened during stadials (cold DO events) and H events, although the mechanisms responsible for these teleconnections remain unknown.

[3] The intensification of the OMZ occurs as a result of higher primary production and/or less oxygen supplied through oceanic ventilation. Several studies, conducted along the American margin within the northeastern Pacific Ocean, display evidence for a reduction in exported biogenic fluxes [*Dean et al.*, 1997; *Hendy et al.*, 2002; *van Geen et al.*, 2003; *Hendy et al.*, 2004; *Ivanochko and Pedersen*, 2004; *Ortiz et al.*, 2004; *Hendy and Pedersen*, 2005; *Dean et al.*, 2006; *Hendy and Pedersen*, 2006; *Dean*, 2007], and of a higher pore water oxygen content during cold periods (last glacial maximum (LGM) and stadials) [*Dean et al.*, 1997; *Cannariato and Kennett*, 1999; *van Geen et al.*, 2003; *Hendy et al.*, 2004; *Ivanochko and Pedersen*, 2004; *Hendy and Pedersen*, 2005; *Dean et al.*, 2006; *Dean*, 2007; *Nederbragt et al.*, 2008]. Based on a simple advection-diffusion model, calibrated with chlorofluorocarbons, both ventilation and productivity changes are suggested to have had a strong impact on the dissolved oxygen content in the present northeastern Pacific Ocean [*van Geen et al.*, 2006]. In fact, a

[1]CEREGE, Aix-Marseille Université, CNRS, IRD, College de France, Technopole de l'Arbois, Aix en Provence, France.

0883-8305/11/2011PA002126

lower organic carbon content within the sediments during cold events can be explained by either reduced productivity linked to weaker coastal upwelling [*Hendy et al.*, 2004; *Ortiz et al.*, 2004; *Dean et al.*, 2006], and/or by better oxygenation of the water column due to enhanced ventilation [*Zheng et al.*, 2000; *Hendy et al.*, 2004; *Ivanochko and Pedersen*, 2004; *Hendy and Pedersen*, 2005; *Dean*, 2007].

[4] Our study sought to evaluate the relative importance of productivity and ventilation changes as the processes responsible for modulating the past variability of the northeastern Pacific OMZ on glacial/interglacial, as well as H-DO timescales. For this objective, we selected core MD02–2508 (MD08; 23°27.91′N, 111°35.74′W, 606 m water depth, Figure 1), retrieved from the northern limit of the present OMZ within the Eastern Tropical North Pacific (ETNP). The core's location is highly sensitive to changes in productivity and ventilation, and thus to OMZ extension and intensity through time.

[5] In this work, we present a geochemical data set that includes a decadal-resolution elemental analyses of the

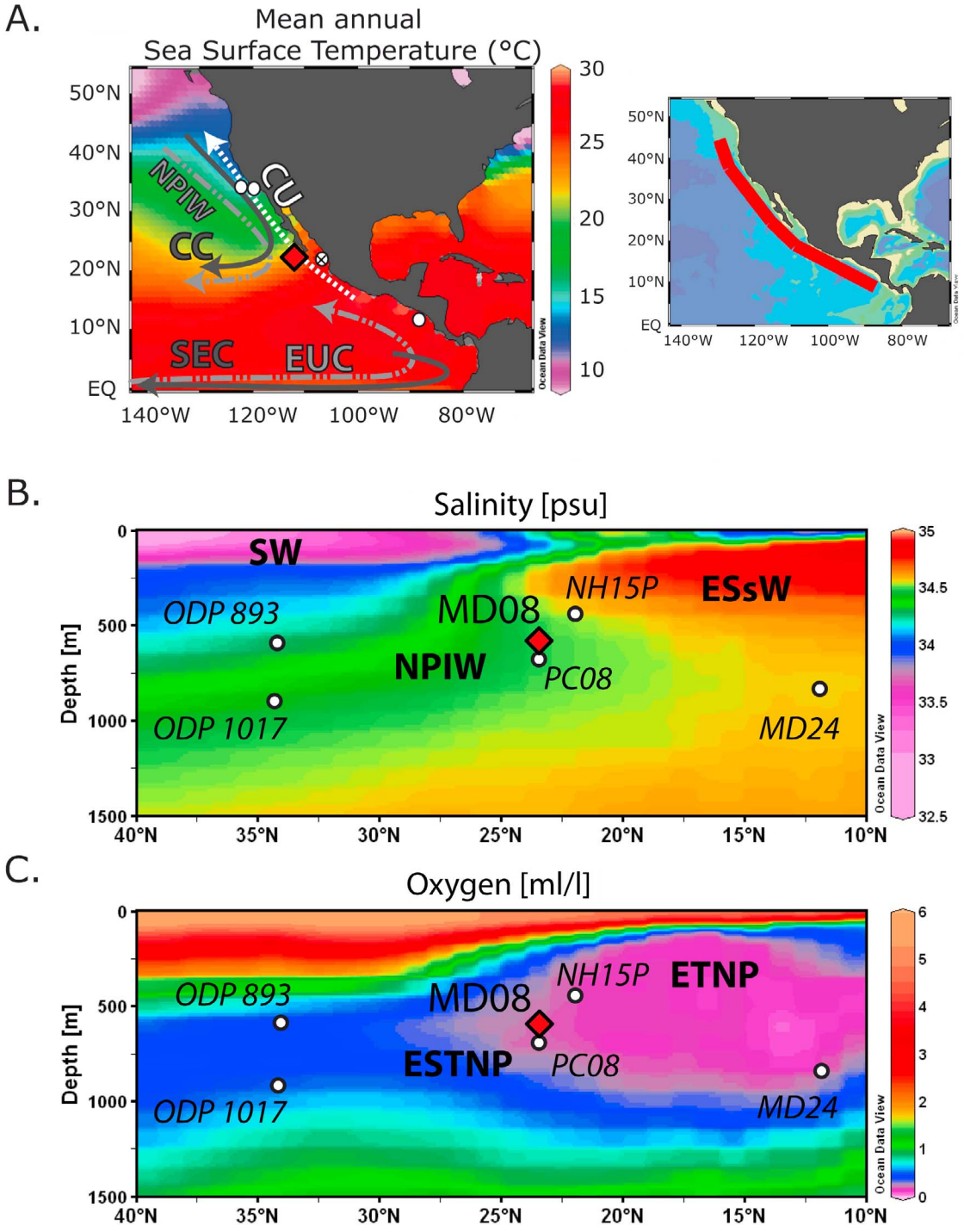

Figure 1

sediment (detrital fraction, carbonates, and organic matter, as well as some redox-sensitive elements) obtained using an X-ray fluorescence (XRF) core scanner, and the concentrations of a series of redox sensitive trace elements measured using an Inductively Coupled Plasma Mass Spectrometer (ICP-MS). We focused our attention on two categories of trace elements that become insoluble under oxygen-depleted conditions in the sediment - elements whose dissolved concentration in the water column is "nutrient-like" (e.g., Cd, Cu, and Ni) and elements whose dissolved concentration is conservative (e.g., U and Mo). If the water column is sufficiently depleted in dissolved oxygen (such as in the OMZ), "nutrient-like" elements are preserved in the sediments and expected to indicate export production (see section 3.2 for detail); whereas conservative elements are expected to essentially vary with the pore water oxygen content, which reflects the bottom water oxygen concentration and local export production [*Calvert and Pedersen*, 1996; *Nameroff et al.*, 2002; *Algeo and Maynard*, 2004; *Tribovillard et al.*, 2006]. Using a statistical analysis, we attempt to separate the effect of export production and bottom water oxygenation in order to provide information on the mechanisms linking high and low latitude climate. The proposed mechanisms are discussed herein by comparing our results to other proxy records and modeling studies.

2. Modern Hydrographic Settings and Productivity

[6] Surface and subsurface oceanography within the eastern North Pacific Ocean margin is mainly driven by the California Current System (Figure 1a), the northeastern section of the North Pacific Gyre [*Tomczak and Godfrey*, 2003]. The California Current (CC) transports the cool and fresh water mass, referred to as Subarctic Water (SW) [*Durazo and Baumgartner*, 2002], southward along the North American margin from Vancouver Island (50°N) to 25°N, and then turns westward off Baja California (World Ocean Atlas 2005 [*Hickey*, 1998]). SW occupies the upper 300 m of the water column within the northeastern Pacific Ocean, and is characterized by low salinity (32.5 to 34.0 psu) (Figure 1b). As a result of active renewal, SW also displays a high oxygen content (5 mL/L, [*van Geen et al.*, 2006]) (Figure 1c).

[7] From the lower limit of the CC down to approximately 1000 m, North Pacific Intermediate Water (NPIW) occupies the water column along the California margin [*Durazo and Baumgartner*, 2002]. NPIW is formed by intense cooling and sea ice formation within the Okhotsk and Bering Seas [*Talley*, 1991; *Takahashi*, 1998; *Shcherbina et al.*, 2003] and flows equatorward to approximately 20°N where it turns westward [*Hendy and Kennett*, 2003, references therein], and then mixes with Equatorial Subsurface Waters ((ESsW) see below; Figure 1b) [*Durazo and Baumgartner*, 2002]. The oxygen content of NPIW decreases from the source area toward the eastern tropical Pacific Ocean, due to organic matter degradation and mixing with highly oxygen-depleted ESsW. All of these processes contribute to the formation of an OMZ at intermediate water depths (500–1000 m, Figure 1c) within the Eastern Subtropical North Pacific (ESTNP) [*Paulmier and Ruiz-Pino*, 2009].

[8] South of 20°N, the water properties at intermediate water depths (100–700m) are very different from those of northern water masses as a result of a southern origin [*Hendy and Kennett*, 2003; *Bostock et al.*, 2010, and references therein]. AntArctic Intermediate Water (AAIW) combined with SubAntarctic Mode Water (SAMW), is formed at southern high latitudes and spreads over the South Pacific Ocean [*McCartney*, 1977]. A positive evaporation/precipitation balance in the central South Pacific Ocean increases surface and subsurface water salinity. The water mass then zonally crosses the Pacific Ocean basin via the Equatorial Under-Current (EUC) and reaches the Central American coast while mixing with northern component water. The resulting ESsW (34.5 to 35.0 psu) [*Durazo and Baumgartner*, 2002] that mixes with upwelled North Pacific deep water corresponds to "Southern Component Intermediate Water," as referenced by *Hendy and Kennett* [2003]. The oxygen content of ESsW is highly depleted (0.2mL/L) below 100 m between 10°N and 25°N, as a result of its distance from the formation zone, high productivity along its pathway (equatorial and coastal upwelling), and slow ventilation. The upper ETNP OMZ corresponds to the ESsW (Figure 1c) [*Paulmier and Ruiz-Pino*, 2009]. Denitrification occurs in the upper water column within the ETNP and increases the $\delta^{15}N$ of residual nitrate within the ESsW [*Voss et al.*, 2001; *Pichevin et al.*, 2010].

[9] ESsW is transported northward along the margin off Baja California by the California Undercurrent (CU, Figure 1a) within subsurface water (roughly 200–300m [*Hickey*, 1998; *Pierce et al.*, 2000; *Durazo and Baumgartner*, 2002; *Pérez-Brunius et al.*, 2006; *Gay and Chereskin*, 2009]). Despite the fact that the CU has been identified to have a nearly continuous flow between the Santa Barbara Basin

Figure 1. Mean annual SST and a simplified map of surface and intermediate depth currents (a). Surface currents are indicated with dark gray arrows (CC for the California Current, SEC for the South Equatorial Current), whereas the current and flow direction of the water mass at intermediate depths are shown with light gray arrows (EUC for the Equatorial Under-Current, NPIW for North Pacific Intermediate Water). Coastal subsurface currents are indicated with a white arrow (CU for the California Undercurrent). The position of core MD02–2508 (red diamond) and the cores discussed in the text (white dots) are also indicated. The white dot filled with a cross corresponds to the NH15P core and the sediment trap study by [*Nameroff et al.*, 2002]. (b) The salinity and (c) the oxygen content from oceanographic transects taken along the North American margin (100 km wide, right upper panel). Major water masses are displayed in Figure 1b as follows: SW for Subarctic Waters transported with CC and ESsW (for Equatorial Subsurface Water). The position of the OMZ in the Eastern Tropical North Pacific (ETNP) and the Eastern SubTropical North Pacific (ESTNP) are shown in Figure 1c. Figure 1 was generated using the Ocean Data View software (http://odv.awi.de) from the World Ocean Atlas 2005 data set (http://www.nodc.noaa.gov/OC5/WOA05/pr_woa05.html).

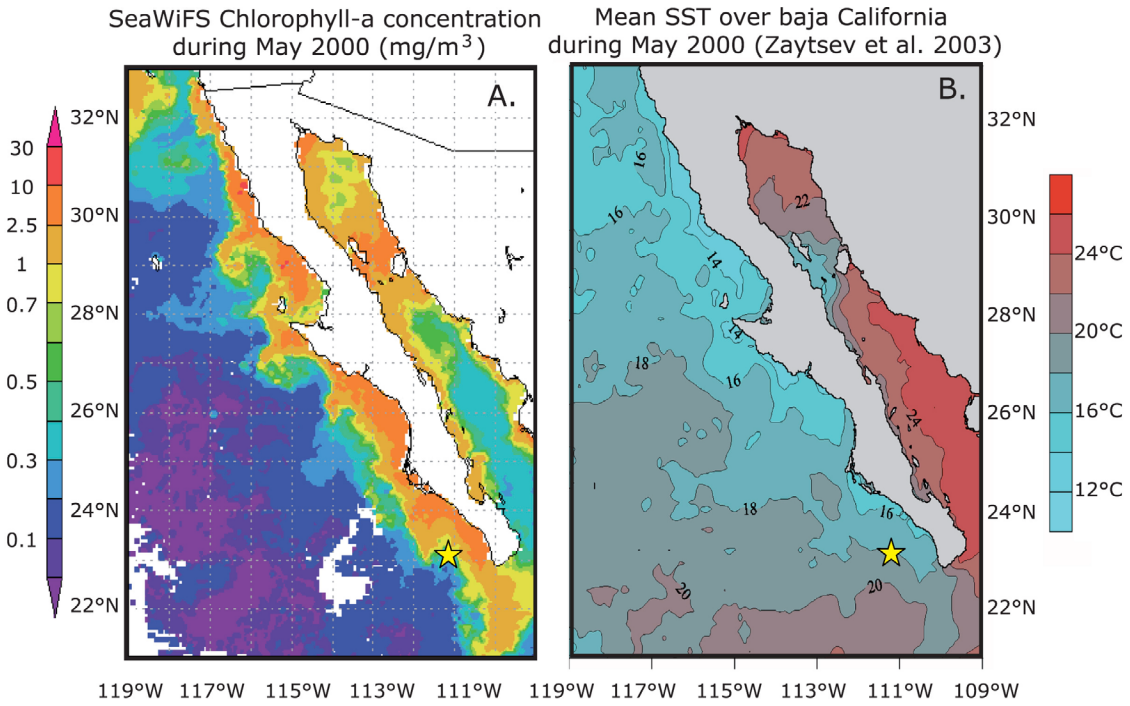

Figure 2. (a) The Seawifs chlorophyll-a concentration (mg/m^3) estimation for May 2000 for Baja California (http://reason.gsfc.nasa.gov/Giovanni/). The analyses and visualizations provided in Figure 2a were produced using the Giovanni online data system, developed and maintained by the NASA GES DISC [*Acker and Leptoukh*, 2007]. (b) The mean SST for Baja California during May 2000 [*Zaytsev et al.*, 2003]. The core MD02–2508 site is indicated with a yellow star.

(34°N) and 50°N [*Pierce et al.*, 2000], CU behavior is not well-known off Baja California. Worth noting is that the water mass transported by the CU (derived from ESsW) may be the main nutrient source during coastal upwelling at the core site [*Durazo and Baumgartner*, 2002; *Ladah*, 2003] and displays high δ^{15}N due to denitrification within the northern extent of the ETNP [*Kienast et al.*, 2002].

[10] The MD08 core site is situated below the northern end of the ETNP subsurface (100–500 m) OMZ corresponding to ESsW, and within the intermediate depth ESTNP OMZ (500–1000m), corresponding to NPIW (Figure 1c). As a result, the MD08 core site is highly sensitive to ventilation variations both within subsurface and intermediate water depths.

[11] Off Baja California margin, maximum surface productivity occurs during spring and early summer [*Thomas et al.*, 2001] when intense southward winds induce coastal upwelling [*van Geen and Husby*, 1996; *Zaytsev et al.*, 2003]. During May, the typical high-productivity season for Baja California, the distribution of chlorophyll-a in surface water (greater than 10 mg/m^3) correlates to that of low sea surface temperature (SST, 14°C to 16°C) along the coast (Figure 2). In general, productivity between 40°N and 20°N along the western American margin is higher during early summer [*Thomas et al.*, 2001] since the North Pacific Ocean's high pressure cell strengthens and the continental low deepens. The resulting east-west pressure gradient induces stronger equatorward winds that favor enhanced upwelling. In contrast, during winter, the North Pacific High weakens while the Aleutian Low strengthens and extends southward, reducing the east/west pressure gradient and associated upwelling.

3. Materials and Analytical Strategy

3.1. Materials and Age Model

[12] Core MD02–2508 was collected from the continental slope off the south Baja California peninsula by the *R.V. Marion-Dufresne* during the coring campaign MD126-MONA (IMAGES VIII, summer 2002). At present, the core site is located within oxygen depleted NPIW (Figures 1b and 1c).

[13] Sediment within the core consisted of hemipelagic silty clayey muds containing biogenic and mineral fractions. Several intervals displayed millimetric to centimetric scale laminations composed of light colored biogenic remains and dark-colored organic matter and terrigenous sediment [*Blanchet et al.*, 2006] (Figure 3). Physical properties measured aboard indicated that lithologic changes are associated with color and density characteristics, with the dark, organic-rich laminae exhibiting lower density (Figure 3) [*Beaufort et al.*, 2002; *Blanchet et al.*, 2007].

[14] The age model was first developed using fourteen ^{14}C dates determined from the benthic foraminifer *Uvigerina peregrina*, two dates determined from the planktonic foraminifera *Globigerinoides ruber*, and the Blake magnetic excursion [*Blanchet et al.*, 2007]. In order to refine this chronology and to develop a more accurate age model with respect to Greenland climate variations, we used a visual correlation of the wet bulk density (WBD) obtained from the GEOTEK logger and the lightness (L*) obtained by spec-

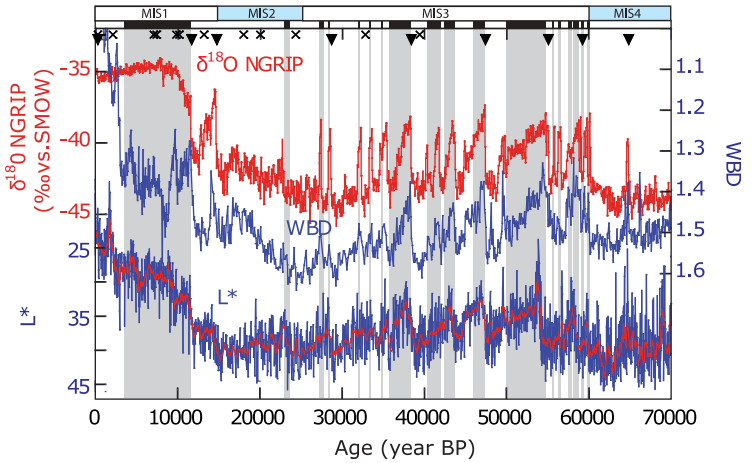

Figure 3. The isotopic composition of the north GRIP ice core (δ^{18}O‰/SMOW) based on the SS09sea time scale [*Johnsen et al.*, 2001], the wet bulk density (WBD), and the lightness (L*) of core MD02–2508 [*Beaufort et al.*, 2002]. Black triangles indicate the position of the tie points used for building the age model. Crosses indicate intervals dated by ^{14}C (see text). Gray vertical bars indicate laminated intervals [*Blanchet et al.*, 2007].

trophotometry [*Beaufort et al.*, 2002] as compared to the NGRIP isotopic oxygen record (based on the SS09sea time scale [*Johnsen et al.*, 2001]) (Figure 3). Based on our current knowledge, such layers of OMZ sediments are generally formed during warm periods (section 1) [cf. *Dean et al.*, 2006; *Dean*, 2007]. Indeed, off the Baja California margin at a site very close to the MD08 location (core PC08, Figures 1b and 1c), physical properties of the sediments, such as the diffusive spectral reflectance (an indicator of the organic carbon content), were used to successfully build an accurate age model with respect to the Greenland ice core isotopic record [*Ortiz et al.*, 2004; *Marchitto et al.*, 2007]. Cores MD08 and PC08 have very similar trace element contents and variabilities (section 4.2) indicating an equivalent sedimentation regime.

[15] Additionally, the new age model presented here shows reasonable agreement to the age model of *Blanchet et al.* [2007], supporting the validity of our dating approach with an offset smaller than 2 kyr for the last 40 kyr B.P. and 5 kyr between 40 kyr and 70 kyr B.P. The estimated sedimentation rate was approximately 43 cm/kyr during the Holocene, decreased to 15 cm/kyr during the LGM, and was between 20 and 50 cm/kyr during Marine Isotope Stage (MIS) 3 (auxiliary material).[1] Laminated intervals correspond to interstadial periods within the Greenland ice core (Figure 3).

3.2. Analytical Strategy

[16] In order to distinguish between changes in oxygen concentration caused by biological production as opposed to ocean ventilation we used a series of trace element records. Trace elements, for which the dissolved concentration profile is nutrient-like, such as Cd, Cu, and Ni, are considered to be associated with marine organic matter since they are incorporated into the particulate organic fraction during growth or scavenged by the organic phase, in particular humic or fulvic acids [*Nameroff et al.*, 2002; *Algeo and Maynard*, 2004; *Tribovillard et al.*, 2006]. During organic matter degradation within the water column and within the sediment, these elements are released into seawater and pore water. Oxygen depletion in the water column minimizes remineralization of the organic fraction [*Guidi et al.*, 2008]. A low oxygen content within the water column, and a high export production produces a depletion of dissolved oxygen in pore water. Under such pore water conditions, these elements would be preserved in sediments in insoluble forms (e.g., sulfides) and can be used as an indicator of export production [*Calvert and Pedersen*, 1993, 1996; *Tribovillard et al.*, 2006; *Calvert and Pedersen*, 2007]. Note that we use the term "export production" for the carbon and nitrogen component of organic matter (R^2 = 0.94 between C and N, data not shown) that reaches the seafloor, excluding the phosphorous fraction for which no data is available.

[17] The behavior of U and Mo is different from the "nutrient-like" elements because they are not directly involved in the biological cycle. Their accumulation in sediments is essentially controlled by the oxygen content of pore water that is, in turn, determined by bottom water oxygenation and local organic rain (see an example with *Pailler et al.* [2002]). In suboxic pore water ([O_2] between 2ml/l and 0.2ml/l), soluble U(VI) is reduced to highly insoluble U(IV) that precipitates and accumulates in the sediment via diffusion across the water/sediment interface. U accumulation may be promoted by the kinetic effect, in areas of low sedimentation rates [*Klinkhammer and Palmer*, 1991; *Algeo and Maynard*, 2004; *Tribovillard et al.*, 2006]. Molybdenum precipitates in pore water as insoluble sulfides under anoxic conditions ([O_2] < 0.2ml/l) in the presence of free H_2S. The diffusion of dissolved Mo from oxic/suboxic bottom water toward anoxic pore water maintains the precipitation and favors enrichment in the sediment, although Mo scavenging by organic matter and/or Mn oxides from the water column can also contribute to the accumulation [*Shimmield and Price*, 1986; *Tribovillard et al.*, 2006].

[1] Auxiliary materials are available in the HTML. doi:10.1029/2011PA002126.

[18] Arsenic, V, and Cr display a mixed feature for the two categories. Arsenic accumulation in sediment is mainly linked to diffusion from the overlying waters and the trapping of pyrite or other sulfide phases [*Böning et al.*, 2004]. Dissolved V and Cr generally display a conservative behavior in an oxic water column, but can be scavenged onto organic matter in an anoxic water column and trapped in anoxic sediment [*Böning et al.*, 2004; *Tribovillard et al.*, 2006]. Since the affinity for binding to organic matter and the sensitivity of pore water oxygenation are different for each trace element, it should be possible to separate the impact of biological production and pore water oxygenation.

[19] Such a simplified interpretation of trace element behavior for the Baja California region was validated by data obtained from a previous study of the modern biogeochemical cycles in the water column and in the sediment [*Nameroff et al.*, 2002]. A series of trace elements was analyzed in seawater, material from sediment traps, and sediment samples collected just south of Baja California within the present OMZ (23.5°N, 106.5°W, near core site NH15P, Figure 1). Dissolved Cd displayed a nutrient-like profile, while the Cd content in particulate material was characterized by a strong enrichment relative to the lithogenic fraction, with a similar pattern to TOC. Particulate Cu displayed a gradual increase with water depth, likely reflecting continuous scavenging onto organic matter [*Boyle et al.*, 1977; *Tribovillard et al.*, 2006]. Dissolved U, Mo, and V in the water column displayed conservative profiles, whereas U and V values in settling particulate material were not enriched as compared to the lithogenic fraction. The results support the assumption that any U and V enrichment in the sediment is essentially related to anoxic/suboxic conditions in pore water. Therefore, Cd, Ni, and Cu were clearly associated with the settling particulate organic fraction, while U and Mo accumulation was mainly linked to pore water oxygenation.

3.3. Bulk Sediment Chemistry

[20] Quantitative bulk sediment chemistry was analyzed at 10 cm resolution (corresponding roughly to 500 years) with an ICP-MS (Agilent 7500ce) at CEREGE. Approximately 160 samples of well-homogenized freeze-dried sediment (30 mg) were dissolved in a mixture of ultrapure acids (0.6 mL of 15M HNO_3 and 0.3 mL of 22M HF) using a microwave (CEM Mars 5) digestion procedure. In order to assess the accuracy of the measurements for all of the elements analyzed (Al, Ti, Fe, Mn, Ca, Sr, V, Cr, Ni, Cu, As, Mo, Cd, and U), we digested and analyzed geostandards that spanned the concentration range of our samples: MAG-1 (marine mud), BE-N (basalt), and GSD12 (river sediment). The estimated analytical uncertainty was less than 5%. Blank levels for the total digestion procedure were lower than 2% of the mean measured concentration for all of the elements.

[21] In order to capture the rapid variability of elemental composition, high resolution XRF measurements for Ca, Sr, Ti, Fe, and Br were performed on the archived portion of the split sediment core at CEREGE using a core scanner (ITRAX, COX Analytical Systems). A Mo X-ray source was used at 30 kV and 45 mA, with a 15 s counting time. Depending on the lamination thickness, the spatial resolution of the measurements was between 200 μm and 0.5 cm (corresponding to the decadal time scale).

[22] The total organic and inorganic carbon content of the core can be found in the work given by *Blanchet et al.* [2007]. Briefly, the bulk sediment carbonate content was determined from the total and organic carbon content in bulk sediment using a FISONS NA 1500 elemental analyzer. Once the total carbon was analyzed, the carbonate was removed with 1M HCl. The uncertainty associated with the carbonate and nitrogen content obtained using this method is estimated to be ~3% (1σ) [*Pailler and Bard*, 2002; *Blanchet et al.*, 2007].

4. Results

4.1. High Resolution Measurements of Major and Minor Elements for the Last 70 kyr

[23] Bromine, Ti, Cl, Ca, Sr, Fe, and Mn were measured using XRF in order to determine the rapid variability of TOC, the terrigenous fraction, carbonates, and redox conditions. The Br content of marine sediment can be used as a proxy for TOC, although part of the Br signature is also related to the pore water content [*Croudace et al.*, 2006; *Mayer et al.*, 2007; *Ziegler et al.*, 2008]. A best fit between the Br intensity and TOC was obtained using a logarithmic relationship (R^2 = 0.85, Figure 4a) rather than a linear relationship. The log-relationship is likely formed by the fact that sediment rich in TOC is more porous and part of the Br signal is derived from pore water. Since the variability in the Br/Cl ratio (here Cl is an indicator of pore water) was similar to that of the Br intensity, we used the logarithmic relationship in order to convert the Br intensity to the TOC content (Figure 4a).

[24] Br-based TOC varied between 5 and 15% for the past 70 kyr, with the highest values occurring during the Holocene (10 to 15%) and the lowest values occurring during MIS2 and the late MIS3 (5 to 8%, Figure 4a). Millennial to centennial scale variability (between 5 and 10%) was superimposed on this long-term trend, with higher values occurring within laminated intervals (corresponding to warm DO events, Figure 3). Lower values were observed for bioturbated intervals (corresponding to H events and stadials).

[25] In addition to Br, the intensity ratio of Compton scatter (incoherent) to Rayleigh scatter (coherent) as obtained from XRF measurements displayed a similar variability to TOC, with higher values for laminated layers (Inc/Co, Figure 4a) since Compton scatter is inversely proportional to the mass absorption coefficient of the sample. The ratio represents the variations of the relative proportion of light to heavy elements [*Croudace et al.*, 2006], and is, therefore, a semi-quantitative indicator of organic matter.

[26] In order to monitor millennial scale terrigenous fraction variability, we used the XRF-based Ti content (Figure 4a). Although Al is often utilized as a terrigenous indicator, the XRF analysis of this element within wet sediments is highly influenced by the pore water content [*Tjallingii et al.*, 2007]. Our approach was supported by a tight correlation between the Al and Ti concentrations obtained using ICP-MS (R^2 = 0.95, Figure 4a). Over the studied period, the Al concentration ranged between 2 and 5%, whereas the Ti concentration ranged between 1000 and

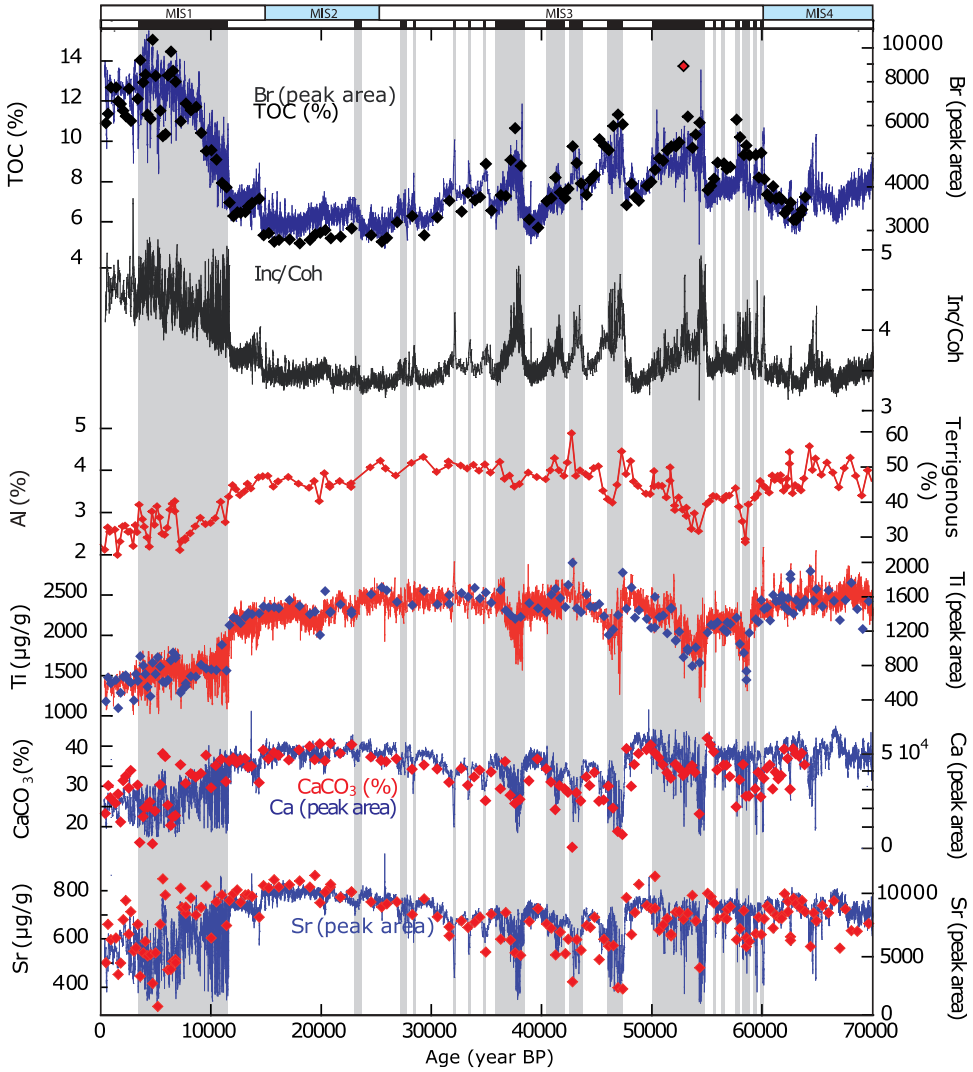

Figure 4a. The relative abundance of Br, Ti, Ca, and Sr (peak area), and the ratio between incoherent and coherent scattering for core MD02–2508 over the past 70 kyr obtained using the XRF core scanner. Concentrations of Al (%), Ti (μg/g), and Sr (μg/g) were obtained from ICP-MS measurements, whereas TOC and $CaCO_3$ concentrations (%) were obtained using a CNS elemental analyzer (*Blanchet et al.*, 2007). Gray vertical bars indicate laminated intervals. The high TOC content (red diamond) corresponds to the anomalously high C/N ratio (16.5 [*Blanchet et al.*, 2007]) that is possibly related to the contribution of continental organic carbon. The relationship between the Br intensity and the TOC used here is, as follows: TOC (%) = 7.5446 * Ln(Br intensity) - 54.837.

2500 μg/g. By assuming that the Al concentration in the terrigenous phase was constant and equal to the value for the Upper Continental Crust (UPC, 8%), [*McLennan*, 2001], we determined that the terrigenous fraction accounted for between 30 and 60% of bulk sediment (Figure 4a). The Ti XRF intensity displayed lower values within laminated intervals, during the Holocene, and for the beginning of MIS3, while the highest content occurred between 20 and 50 kyr B.P. and during MIS4 (Figure 4a).

[27] Ca XRF counts (1,000 to 70,000 in peak area) were correlated to carbonates obtained using a CNS analyzer (R^2 = 0.6), and displayed a negative correlation with TOC on a millennial time scale (Figure 4a). The Ca content obtained by ICP-MS analysis was in agreement with the $CaCO_3$ content that ranged from 14 to 42% for the entire record, with the lowest value occurring during the Holocene and during laminated intervals of MIS3 (Figure 4a). The similarity between Sr and Ca indicates that most of the Sr was from carbonates (Figure 4a).

[28] By using Ti as a terrigenous indicator, we examined the Mn/Ti and Fe/Ti ratios obtained from an XRF scan and ICP-MS measurements as redox indicators (Figure 4b). Mn/Ti ratios were approximately uniform around 0.075 g/g for the entire period studied, and were much lower than the terrigenous reference of 0.12 g/g (see details within the caption of Figure 4b). The result suggests that Mn oxides were lost from the sediment [*Nameroff et al.*, 2002, 2004] and that the pore water was never completely oxic at the MD08 core location during the period studied. In contrast, the Fe/Ti ratio ranged from 9 to 11 g/g, which is higher than the estimated terrige-

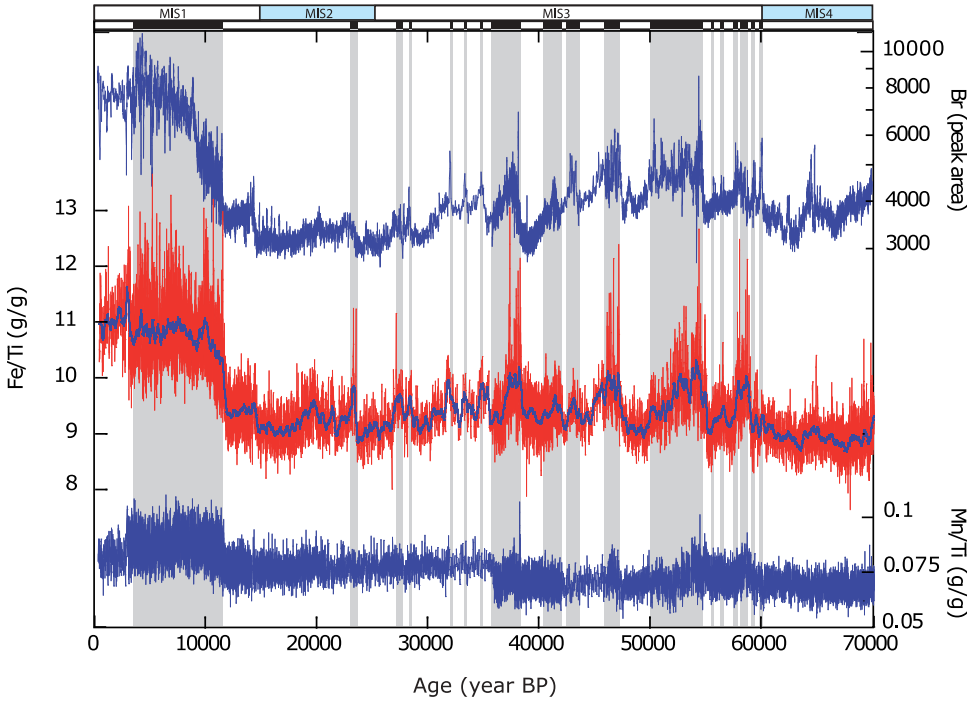

Figure 4b. The bromine intensity obtained by XRF, and the calibrated Fe/Ti ratios and Mn/Ti ratios (g/g) obtained using a combination of XRF and ICP-MS measurements. The blue line shown on the high resolution Fe/Ti corresponds to a 250 year running mean. The gray vertical bars indicate laminated intervals. Since the Ti content within terrigenous material may vary with grain size, we evaluated the lithogenic elemental ratio by combining the composition of the Upper Continental Crust (UPC) with the Al/Ti ratio obtained from core MD08, as follows: $M/Ti_{(ref)} = M/Ti_{(UPC)} * \text{mean } Al/Ti_{(MD08)}$. The calculated lithogenic reference was 7g/g for Fe/Ti and 0.12g/g for Mn/Ti.

nous reference (7 g/g). Additionally, the Fe/Ti ratio varied with the Br intensity, with higher values found for the Holocene and for glacial laminated intervals, possibly due to the formation of pyrite under reducing conditions.

4.2. Trace Element Variability for the Past 70 kyr

[29] All of the trace elements analyzed for this study (V, Cr, Ni, Cu, As, Mo, Cd and U) displayed similar patterns to Br-based TOC, with higher concentrations in laminated layers and lower values in bioturbated layers (Figure 4c). Element/Al ratios were much higher than the respective ratios for the UPC and displayed close variability to the respective elemental content on glacial/interglacial and millennial scales during MIS 3 (Figure 4c). For example, Cu ranged between 50 and 80 μg/g, with higher values during the Holocene (60 to 80 μg/g) and lower values during late MIS3 and MIS2 (around 50 μg/g, Figure 4c). Millennial scale variations were superimposed onto this trend with higher values found within some of the laminated intervals. The Cu/Al ratio (roughly 2×10^{-3} g/g) was nearly ten times higher than the UPC ratio (3.1×10^{-4} g/g [*McLennan*, 2001]). Cadmium had a baseline at 2 μg/g and peaks that reached concentrations of 15 μg/g within laminated layers and during the Holocene. The Cd/Al mean ratio (approximately 2×10^{-4} g/g) was more than one hundred times higher than the UPC ratio (1.2×10^{-6} g/g). Cu/TOC and Cd/TOC ratios at the core top (700 and 50 μg/g, respectively) were similar to the respective value in settling particulate material (approximately 650 and 30 μg/g, respectively) [*Nameroff et al.*, 2002], indicating that enrichment of Cu and Cd was essentially associated with organic matter.

[30] The U content within MD08 sediment was between 7 and 25 μg/g (Figure 4c), and again, the mean U/Al ratio (4×10^{-4} g/g) was more than ten times higher within MD08 sediment than in the UPC (3.5×10^{-5} g/g). Furthermore, the U/TOC ratio within Holocene sections of the core (1×10^{-4} g/g) was approximately five times higher than that within sediment traps [*Nameroff et al.*, 2002]. The Mo/Al ratio within MD08 sediment ranged between 1.0×10^{-4} g/g and 2.0×10^{-3} g/g, indicating a strong enrichment as compared to the UPC value (0.19×10^{-4} g/g). The Mo/TOC ratio (200 μg/g) was much higher than within settling particulate material (50 μg/g [*Nameroff et al.*, 2002]). Barium, commonly used as an export production proxy, displayed very different variability from other analyzed elements, with a broad peak centered at 7.5 kyr without any clear millennial-scale change (auxiliary material). Since we suspect barite dissolution and dissolved Ba remobilization under reducing conditions [*Schenau et al.*, 2001; *Nameroff et al.*, 2002, 2004], we choose not to use this element in this study.

[31] In general, the similar variability observed for the element/Al ratios and the trace element concentration for core MD08 are a testament to the fact that the observed trace element enrichments were not produced by a change in lithogenic inputs (Figure 4c). Our results are in excellent agreement with measurements performed for Mn, Cd, Cr, Cu, Mo, Ni, and V for the core PC08 site located close to MD08 (Figure 1) [*Dean et al.*, 2006].

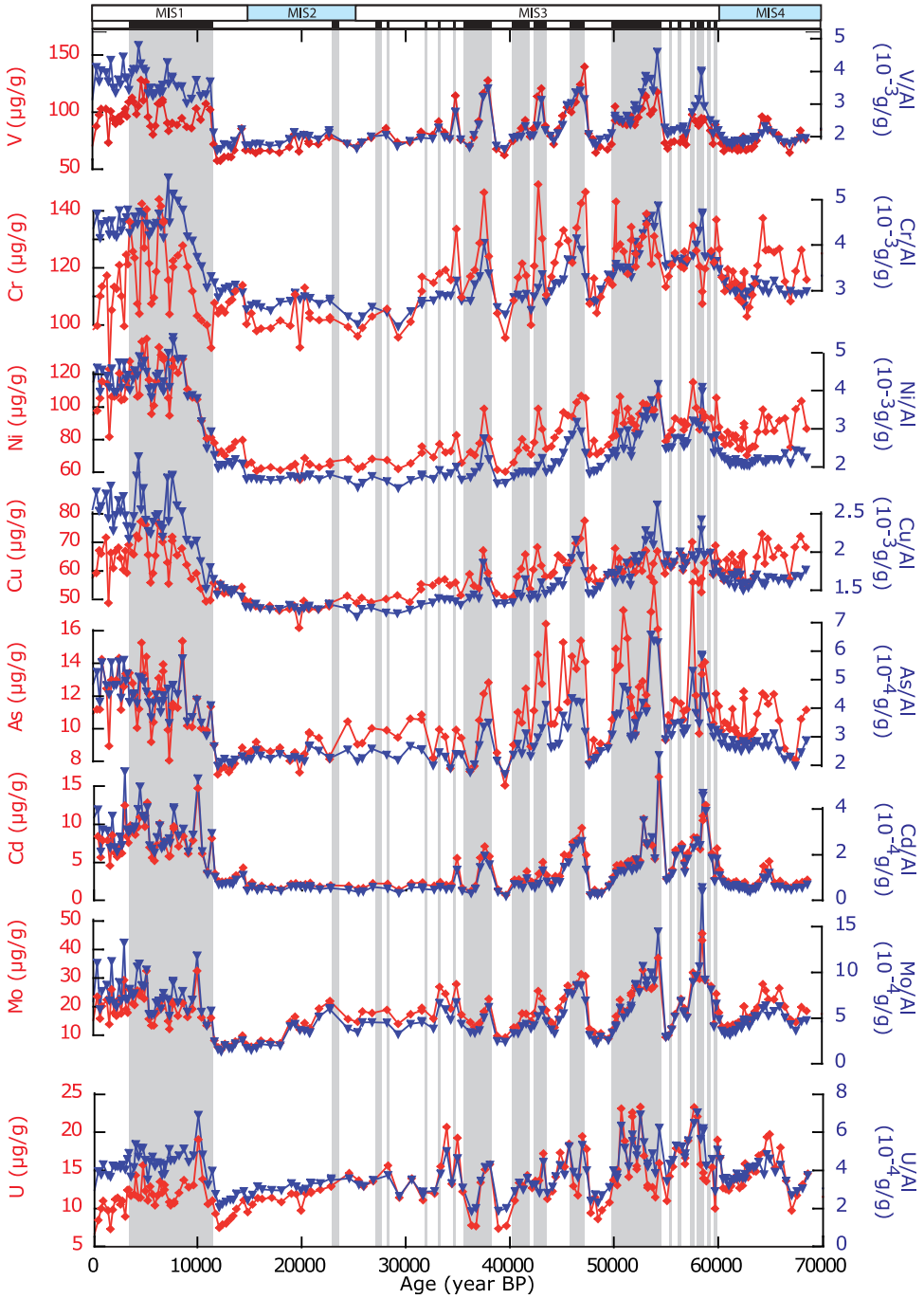

Figure 4c. The bulk sediment concentrations of V, Cr, Ni, Cu, As, Mo, Cd, U, and the respective element/Al ratios. Gray vertical bars indicate the laminated intervals.

4.3. Principal Component Analyses of Element/Al Ratios

[32] In order to extract the dominant modes of variability in relation to their mode of accumulation, we applied a Principal Component Analysis using the AnalySeries software [*Paillard et al.*, 1996] to the element content which was normalized to Al (TOC, $CaCO_3$, V, Cr, Fe, Ni, Cu, As, Sr, Mo, Cd, and U, Table 1). The results indicated that 92% of the total variance could be expressed by three principal components (PC) (Table 1).

[33] The first principal component (PC1, Figure 5a and Table 1), explained 76% of the data set variance, and displayed relatively high loadings (slightly above 0.3) for almost all of the ratios except for the elements linked to carbonates ($CaCO_3$ and Sr with loadings around 0.15), and to pore water oxygenation (U and Mo with loadings of 0.25 and 0.26 respectively, Table 1). PC1 displayed a striking similarity to the TOC/Al and Br-based TOC/Ti ratios (Figure 5a). A strong correlation between trace elements (Cd, Ni and Cu) and TOC (R^2 = 0.67, 0.89, 0.67, respec-

Table 1. The Results of a Principal Component Analyses for the Al-normalized Elemental Ratio in the MD02–2508 Core[a]

	PC1 (0.76)	PC2 (0.11)	PC3 (0.053)
TOC	0.34	−0.01	−0.25
$CaCO_3$	0.14	0.67	0.20
V	0.32	−0.11	−0.14
Cr	0.35	0.00	−0.11
Fe	0.22	−0.07	−0.14
Ni	0.34	0.05	−0.19
Cu	0.34	0.01	−0.21
As	0.32	−0.09	0.02
Sr	0.16	0.65	0.11
Mo	0.26	−0.24	0.30
Cd	0.31	−0.07	0.02
U	0.25	−0.18	0.80

[a]The three principal components were derived from 12 elemental ratios that explained 76% (PC1), 11.4% (PC2), and 5.3% (PC3) of the total variance.

tively) was observed for MD08 and compared well with sediment trap results [*Nameroff et al.*, 2002] indicating that PC1 could represent export production determined by a combination of primary productivity, remineralization at subsurface water depths, and transport processes of particulate matter.

[34] PC2 displayed the highest loadings for $CaCO_3$ and Sr (0.67 and 0.65, respectively; Table 1 and Figure 5b) and was closely related to the carbonate components. Since the carbonates/terrigenous ratio can vary at least partly with both $CaCO_3$ production and preservation, we examined some selected foraminiferal shells from laminated high-organic content intervals (Holocene and interstadials events) using scanning electron microscopy. Some planktonic foraminiferal shells displayed clear evidence of dissolution, in the form of peeled calcite layers and the formation of cracks, as reported by [*Dittert and Henrich*, 2000], indicating that the $CaCO_3$ content within the MD08 core was in part influenced by preservation. However, we could not reliably separate the influence of $CaCO_3$ production/preservation and dilution by the terrigenous fraction in the present data set. As a result, the variability of PC2 associated with the $CaCO_3$ content is not discussed further.

[35] PC3 (Figure 5c and Table 1) explained 5.3% of the data set variance, and U and Mo showed the highest loading (0.80 and 0.30, respectively) (Table 1). On glacial/interglacial timescales, PC3 displayed the highest values during MIS2, and late and early MIS3, whereas low values were seen during MIS1 and mid-MIS3. On a millennial timescale, the lowest values were seen mainly within bioturbated stadial layers. Uranium and Mo are two elements that we considered as indicators of pore water oxygenation. The dissolved oxygen content in pore water varies with the overlying bottom water oxygen content and local export production. Since PC1 represents export production and since part of U and Mo enrichment related to export production was already taken into account in PC1, we concluded that PC3 indicates bottom water oxygenation controlled by oceanic circulation. Consistent with this interpretation, the U/TOC ratio and PC3 displayed a similar variability (Figure 5c). Authigenic U accumulation could have been influenced by a change in the sedimentation rate [*Algeo and Maynard*, 2004; *Tribovillard et al.*, 2006]. A lower sedimentation rate during the LGM (20 cm/kyr), as compared to the Holocene or to early MIS3 values (40 cm/kyr), may have partly contributed to higher PC3 values during the LGM (Figure 5c). However, overall there was a good correlation between PC3 and a previously published record of bottom water oxygenation (ODP 1017 955m [*Cannariato and Kennett*, 1999], see section 5.3), supporting the theory that PC3 represents bottom water oxygenation.

5. Discussion

[36] A principal component analysis performed on core MD08 revealed the presence of two independent components (PC1 and PC3), suggesting that two distinct factors modulated the past intensity and extension of the OMZ off the coast of Baja California.

[37] Important to note is that export production is determined by the interplay between primary production, remineralization in the water column, and the transport processes of particulate matter. Coastal upwelling, which drives productivity, is intimately linked to the shape and angle of the coastline relative to the dominant winds [*Zaytsev et al.*, 2003] that may have changed due to sea level variations [*Giraud and Paul*, 2010]. However, MD08's distance from the shoreline (100 km) likely attenuated the potential influence of any change in the position of major coastal upwelling cells on biogenic matter transport toward the core site. Moreover, the width of the continental shelf above 100 m deep (the typical range for glacial/interglacial sea level change [*Waelbroeck et al.*, 2002]) is approximately a tenth of a kilometer. Therefore, organic matter retention near the coast and transport processes from the coast toward the core site would not drastically change with sea level variations. The overall negative correlation between TOC and terrigenous elements and carbonates indicates that calcitic and terrigenous ballast minerals are not likely responsible for TOC variations within the sediments. Thus, we assumed that vertical transport processes had a minor influence on variations of export productivity.

[38] Below, we discuss the variability of PC1 and PC3 in terms of local export production and bottom water oxygenation, respectively. We compared PC1 and PC3 variability with other paleoceanographic proxy records and modeling experiments in order to clarify the following points: (1) primary productivity, (2) subsurface water oxygenation, and (3) intermediate water oxygenation on millennial and glacial/interglacial timescales. Our final objective is to propose mechanisms that could potentially be responsible for transferring the climate signal from the high northern Atlantic Ocean latitudes to the northeastern tropical Pacific Ocean OMZ.

5.1. Atmospheric-Driven Upwelling Variability and its Impact on Primary Productivity

[39] Our interpretation of PC1 as an export production indicator is supported by low-resolution microfossil assemblages for core MD08 that have indicated reduced productivity during cold periods [*Murdmaa et al.*, 2010]. The benthic foraminiferal abundance in PC08 (Figure 1) also suggested a decrease in export production during DO stadials [*Ortiz et al.*, 2004]. Therefore, proxy records are in agreement, indicating a decrease in primary or export production off Baja California during cold periods on both orbital and millennial timescales.

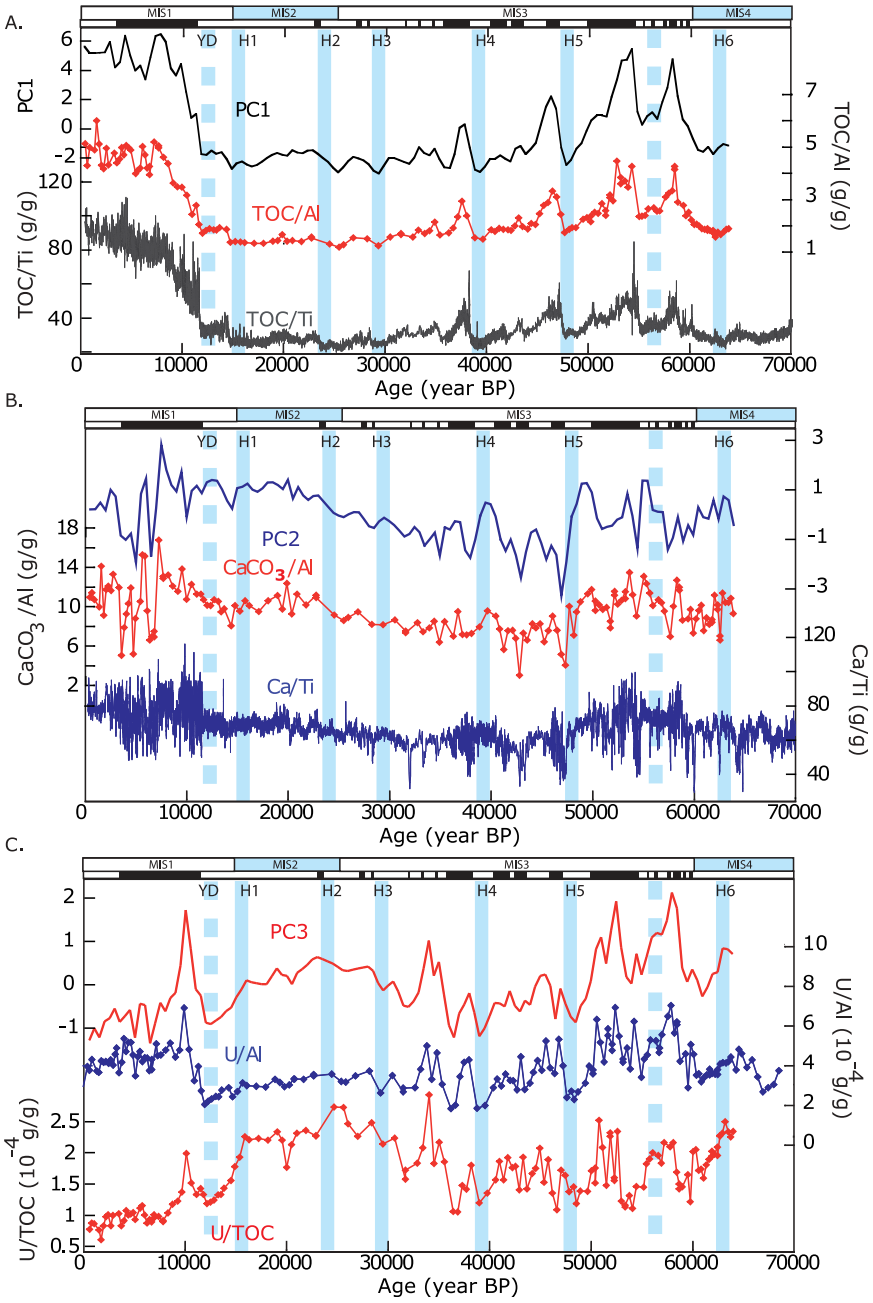

Figure 5. (a) The PC1, the TOC/Al ratios, and the XRF Br based TOC/Ti ratios. The blue vertical bars indicate H events. The top black horizontal line corresponds to the laminated intervals. (b) The PC2, the $CaCO_3$/Al ratios, and the XRF based Ca/Ti ratios. The blue vertical bars indicate H events. The top black horizontal line corresponds to the laminated intervals. (c) The PC3, the U/Al ratios, and the U/TOC ratios. The blue vertical bars indicate H events. The top black horizontal line corresponds to the laminated intervals.

[40] Since wind driven upwelling influences primary productivity not only at the studied site but also along the entire northeastern Pacific Ocean margin [*Thomas et al.*, 2001], we compared the PC1 trend to biological productivity indicators from different cores in this area. On glacial/interglacial timescales, lower glacial productivity was inferred from TOC and carbonates at the ODP1017 core site (34°N, 121.6°W [*Hendy et al.*, 2004]) (Figure 1), and TOC and opal at the NH15P core site (22.4°N, 106.3°W [*Ganeshram and Pedersen*, 1998]) (Figure 1). On millennial timescales, lower primary productivity, based on a reduced planktonic foraminiferal flux (*Globigerinoides bulloides*) [*Hendy et al.*, 2004], was reported during stadials and some H events (H1, H3, H4 and H5) at the ODP1017 site (Figure 6). The results are consistent with PC1, supporting the idea of regional scale productivity changes both on millennial and glacial-interglacial timescales.

[41] What mechanisms could have reduced upwelling during cold periods? During glacial periods, the size and height of the Laurentide and the Cordilleran ice sheets

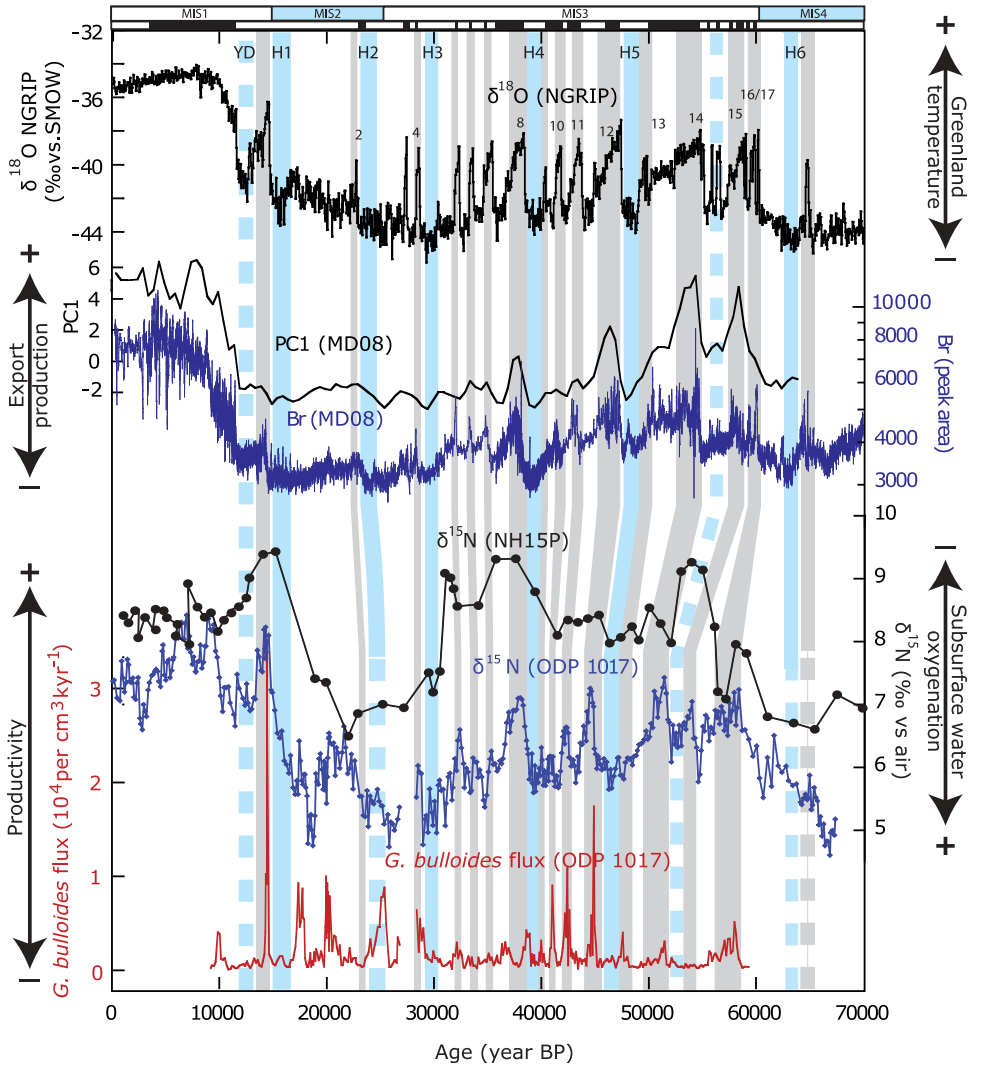

Figure 6. The isotopic composition of the north GRIP ice core (δ^{18}O‰/SMOW) based on the SS09sea time scale [*Johnsen et al.*, 2001], the PC1 and Br counts (this study), the δ^{15}N of the NH15P and ODP1017 cores, and the *G. bulloides* flux in ODP1017 [*Hendy et al.*, 2004]. Gray vertical bars indicate DO warm periods; blue vertical bars indicate H events.

increased drastically [*Benson et al.*, 2003]. Intense cooling and changes in the topography of the region likely favored the establishment of an extended and persistent anti-cyclonic cell over the North American continent [*Kutzbach and Wright Jr.*, 1985; *Romanova et al.*, 2006]. The development of a continental high-pressure cell could have induced weaker southward winds or a wind direction reversal along the northwestern American coast, thus reducing coastal upwelling.

[42] On a millennial timescale, changes in the Cordilleran ice sheet extension [*Benson et al.*, 2003] combined with modification of snow cover over the northwestern American continent, may have had a significant impact on atmospheric circulation, in a manner similar to glacial periods. Indeed, extended high pressure over the northern American continent during stadials is consistent with a southward shift in major midlatitude climate patterns, such as storm tracks and jet streams [*Asmerom et al.*, 2010; *Wagner et al.*, 2010]. Additionally, North Atlantic Ocean cooling during H events was propagated to high and midlatitudes in the North Pacific Ocean via increased westerly winds over the Eurasian continent [*Clement and Peterson*, 2008]. Modeling studies using fresh water perturbations have indicated that cold SST and enhanced eastward winds in the northern Pacific Ocean (30°N–60°N, [*Mikolajewicz et al.*, 1997; *Okumura et al.*, 2009]) were associated with a deepening of the Aleutian Low, which produced a northward wind stress anomaly along the North American margin, reducing coastal upwelling.

5.2. Subsurface Water Column Oxygenation

[43] The decrease in export production during cold periods can be alternatively explained by better oxygenation of the subsurface layer at core MD08, and therefore, to the lower preservation of organic compounds in the water column [*Guidi et al.*, 2008]. The oxygen supplied to subsurface water at the MD08 site could have been modulated by mixing proportion of ESsW and SW (Figure 1) and the dissolved oxygen content of these water masses. In order to trace

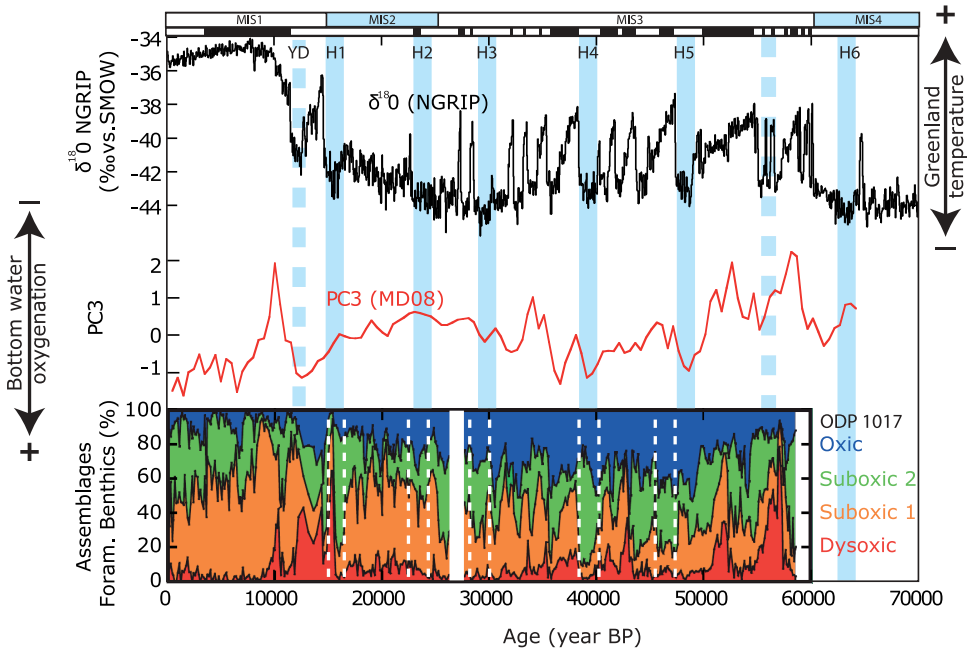

Figure 7. The isotopic composition of the north GRIP ice core (δ^{18}O‰/SMOW) based on the SS09sea time scale [*Johnsen et al.*, 2001], PC3 in MD08 core, and the benthic foraminiferal assemblages within the ODP1017 core [*Cannariato and Kennett*, 1999]. Oxic assemblages indicate bottom water [O_2] > 1.5ml/l, suboxic corresponds to 0.3 < [O_2] < 1.5ml/l, and dysoxic assemblages to [O_2] < 0.3ml/l.

oxygenation conditions at subsurface depth, we used previously published δ^{15}N values recorded for bulk sediments. Sedimentary δ^{15}N from the OMZ reflects the dissolved oxygen content at the subsurface depth and/or local productivity [*Ganeshram et al.*, 2000]. However, further variability can be expected by laterally transported water masses that are characterized by different δ^{15}N values [*Voss et al.*, 2001; *Kienast et al.*, 2002; *Pichevin et al.*, 2010].

[44] During the glacial period (30 kyr to 15 kyr), sedimentary δ^{15}N values from cores NH15P [*Ganeshram et al.*, 2000] (Figure 6) and MD24 [*Pichevin et al.*, 2010], underlying ESsW (Figure 1), were lower than for the Holocene, suggesting reduced productivity and/or a higher oxygen content in the ESsW. In the past, it has been suggested that the northward penetration of a southern water mass within the equatorial Pacific Ocean was promoted during the glacial period [*Herguera et al.*, 2010]. Moreover, the worldwide reduction of δ^{15}N in glacial sediment could be related to increased ventilation in the high latitude Southern Ocean [*Galbraith et al.*, 2004; *Muratli et al.*, 2010]. Therefore, we propose that the subsurface depth at the MD08 site was principally occupied by ESsW, for which the dissolved oxygen concentration was higher than present during the glacial period.

[45] On a millennial timescale, the δ^{15}N record from the ODP1017 site [*Hendy et al.*, 2004] (Figure 1) displayed more oxygenated conditions during H events (H3, H4, and H5) and stadials (Figure 6). Even though this site is located under SW, the sedimentary δ^{15}N record was strongly influenced by the seawater δ^{15}N value of ESsW, since the California Undercurrent transported seawater δ^{15}N signal highly modified by denitrification within the ESsW [*Kienast et al.*, 2002]. Therefore, lower δ^{15}N values for ODP1017 can be interpreted as the higher oxygenation of ESsW during millennial cold events. Alternatively, stronger winds and lower temperatures in the northern Pacific Ocean during H events likely increased the ventilation of SW [*Mikolajewicz et al.*, 1997], and could promote the southward penetration of this well-oxygenated water mass. Thus, better oxygenation at the subsurface depth at the core MD08 site during H events could also be explained by a higher proportion of SW relative to ESsW.

[46] Taken together, biological production and subsurface oxygenation worked in the same manner in reducing export production during glacial and millennial cold periods.

5.3. Millennial Scale Variability in Intermediate Depth Ventilation

[47] One of the most important results obtained from this study was the distinct behavior of intermediate oceanic ventilation on millennial and orbital timescales. On millennial timescale, the PC3 suggested an increase in the oxygen supply to the intermediate water masses in which core MD08 had been bathed during H events (H1, H4, H5, and possibly H3 events, Figure 7). Since core MD08 is presently bathed in NPIW (Figure 1), the millennial-scale bottom water oxygen variability at MD08 may be associated with the active production of NPIW and/or with a greater oxygen content in NPIW during H events. Such a hypothesis is consistent with the variability in benthic assemblages at site ODP1017, also located within the NPIW pathway from the formation zone of this water mass to the MD08 site, which indicates an increased proportion of oxic and suboxic taxa during H events (Figure 7).

[48] What physical processes could have induced the active production of NPIW and/or more oxygen content in NPIW during millennial cold events? The reconstructed SST record from the Okhotsk Sea, the actual NPIW for-

mation zone, displays high amplitude temperature variations with cooler SSTs during stadials [*Harada et al.*, 2006]. Cold SSTs during stadials in the Okhotsk Sea could have enhanced seasonal sea ice formation, leading to increased surface salinity by brine formation. The salinity increase combined with colder SSTs may favor NPIW production. Indeed, several modeling studies have determined an enhanced ventilation at intermediate depths within the North Pacific Ocean during H events [*Saenko et al.*, 2004; *Timmermann et al.*, 2005; *Schmittner et al.*, 2007; *Okazaki et al.*, 2010]. Cooler SSTs and wind induced mixing, which influences North Pacific Ocean subsurface water ventilation (in the subarctic water depth range, cf. section 5.2), could also promote atmospheric oxygen dissolution in the surface NPIW precursor, increasing the dissolved oxygen content in NPIW.

[49] On a global scale, modeling studies indicate the general reorganization of oceanic circulation [*Marchal et al.*, 1998] and a teleconnection between the North Atlantic and Pacific Oceans on a millennial scale. While NADW formation in the North Atlantic Ocean weakened due to fresh water input during H events, salt transport from low latitudes toward high northern latitudes in the Atlantic Ocean was reduced and was diverted toward the North Pacific Ocean through the Southern Ocean [*Saenko et al.*, 2004; *Timmermann et al.*, 2005], and favored intermediate water formation within the northwestern Pacific Ocean. Reduced water vapor transport from the equatorial Atlantic Ocean toward the Pacific Ocean across the Panama Isthmus during H events [*Leduc et al.*, 2007], could further increase salinity within the North Pacific Ocean. As a result, both atmospheric changes in the high latitude North Pacific Ocean and oceanic processes that were triggered in the North Atlantic Ocean, could have contributed to millennial scale variations of ventilation at intermediate depths in the northeastern Pacific Ocean OMZ.

5.4. Reduced Intermediate Depth Ventilation During Late MIS3 and MIS2

[50] In contrast to millennial cold events, PC3 suggested a reduced oxygen content at intermediate depths at the MD08 location (606m) during the glacial period (the late MIS3 and MIS2, Figure 7). At sites ODP893 (576 m, not shown) and ODP1017 (955 m [*Cannariato and Kennett*, 1999]) (Figure 7), a lower oxygen content was suggested by benthic foraminiferal assemblage: the proportion of high dysoxic and suboxic taxa increased in upper intermediate waters (500–1000 m) during the glacial period in the northeastern Pacific Ocean. We propose that this variability is related to a change in the ventilation depth of NPIW. Past studies, based on the carbon isotopic composition of benthic foraminifera, have proposed that glacial NPIW was deeper that today during the LGM (roughly 1000–4000 m as compared to 500–1500 m in the modern ocean [*Keigwin*, 1998; *Matsumoto et al.*, 2002; *Herguera et al.*, 2010]). The modified circulation pattern observed by [*Herguera et al.*, 2010] is consistent with the foraminiferal Cd/Ca ratio record from the northeastern Pacific Ocean, which displayed an opposite ventilation trend between 800 and 1600 m during the last deglaciation [*van Geen et al.*, 1996]. Deep water formation in the North Pacific Ocean during the LGM was also proposed in a recent modeling study [*Okazaki et al.*, 2010], as a response to reduced Atlantic Meridional Overturning Circulation (AMOC). A deeper sinking depth for glacial NPIW (GNPIW) is consistent with a stagnant ventilation within the North Pacific Ocean at depths bathed by modern NPIW, and may explain why H2 and H3 events are only partially evident during late MIS3 and MIS2 at the MD08 core location. However, we acknowledge that the temporal resolution of our record may be too low to resolve these events.

[51] Therefore, an unanswered question is why GNPIW would have sunk deeper in the past than it does under modern conditions, when upper intermediate and subsurface water (ESsW depth range, Figure 1) from a southern origin displays greater oxygenation (cf. Section 5.2.). A possible explanation is that high-latitude North Pacific Ocean surface water once had a higher density as a result of a change in local temperature. Since the LGM is likely the coldest interval of the studied period, an increase in density due to a lower temperature and brine water formation could have had an impact on the GNPIW sinking depth. Additionally, deep water formation within the north Pacific and Atlantic Oceans seems to display a negative correlation [*Saenko et al.*, 2004]. AMOC was reduced during the LGM [*McManus et al.*, 2004; *Curry and Oppo*, 2005] leading to weak ventilation within the Atlantic Ocean below 2000 m, while North Pacific Ocean intermediate ventilation was enhanced below 1500 m but reduced above 1500 m [*Herguera et al.*, 2010]; ventilation within subsurface water of the northeastern tropical Pacific Ocean increased (ESsW depth range, cf. Section 6.2.).

[52] Our results indicate that this pattern, consistent with the Atlantic/Pacific seesaw as described by *Saenko et al.* [2004], was maintained during late MIS3 and MIS2. As a result, the global reorganization of oceanic circulation during the last glacial maximum impacted North Pacific Ocean circulation that was activated and deepened by GNPIW.

[53] Since bottom water oxygenation and export production worked in an opposite manner during late MIS3 and MIS2, the results of this period could provide insight regarding the relative importance of the two factors on OMZ variability. Even though the bottom water oxygen content seems to be lower than at present, the laminated layers are less abundant and the trace element concentrations are generally low (Figure 4c). The observation is in line with the previous study, indicating that high productivity is required to form laminated sediment sequences and to intensify the OMZ [*van Geen et al.*, 2003]. Therefore, we propose that export production is the most fundamental parameter for OMZ variability off Baja California.

6. Conclusions

[54] We studied core MD02–2508 (606 m water depth) retrieved off the coast of Baja California, at the northern limit of the present OMZ in the equatorial North Pacific Ocean, using decadal-resolution XRF measurements (Ca, Sr, Ti, Fe, Br) and a series of trace elements (Cu, Ni, Cd, As, V, Cr, Mo, and U) at a ~500 yr resolution measured using the ICP-MS. The data have allowed us to better constrain the potential mechanisms controlling past OMZ intensity on both millennial and glacial/interglacial timescales.

[55] The Br-based high resolution TOC estimate displayed millennial-scale variability that was very similar to the (DO) and (H) events observed for the $\delta^{18}O$ records of Greenland ice cores, confirming a tight linkage between northern high

latitude climate and the northeastern Pacific Ocean OMZ during the past 70 kyr. All of the trace elements analyzed indicated a very similar pattern to Br-TOC, with higher (lower) values during warm (cold) periods. In addition, U and Mo displayed a broad increase over late MIS3 and MIS2 that was not indicated by other trace elements. Using a principal component analysis, we identified two major factors that explain past OMZ variability off Baja California:

[56] 1. Export productivity was a major factor regulating OMZ intensity, and was determined by the interplay between primary productivity in relation to coastal upwelling and subsurface oxygenation. Based on a comparison with other proxy records and modeling studies, we propose that coastal upwelling was reduced during millennial cold events and glacial periods as a result of reduced southward winds. The subsurface oxygen content is estimated to have been higher during cold periods, either through the contribution of highly oxygenated Subarctic Water during millennial cold events or through an increase in the oxygen content in Equatorial Subsurface Water during the glacial period, as a result of changes within the Southern Ocean. Weaker or smaller northeastern Pacific Ocean OMZ during cold periods are at least partly explained by reduced productivity and enhanced subsurface oxygenation on glacial/interglacial and millennial time scales.

[57] 2. Bottom water oxygenation, as inferred from the PC3, was mostly related to U and Mo variability that was not supported by the export production change. Based on a comparison with other proxy records and modeling studies, we propose better oxygenation of intermediate water during H events by more active North Pacific Intermediate Water (NPIW) formation and/or by an increase in the dissolved oxygen content of this water mass. In contrast, a less oxygenated condition was observed for the late MIS3 and MIS2 as a result of deeper ventilation of glacial NPIW in relation to the global reorganization of oceanic circulation.

[58] **Acknowledgments.** We thank Luc Beaufort (chief scientist), Yvon Balut (IPEV), and the team of the IMAGESVIII-MONA cruise (MD126 North American Margin) on board of *Marion Dufresne*. Marta Garcia was thanked for technical assistance while finishing trace element analyses by ICP-MS. We thank R. Zahn (Editor), H. Bostock, T. Jilbert, A. Paulmier and one anonymous reviewer for their constructive comments that have greatly improve the manuscript. We are grateful to MESR and the Collège de France for providing salary support to O. Cartapanis. Paleoclimate work at CEREGE is supported by grants from the Collège de France, the Comer Science and Education Foundation, the CNRS (LEFE-EVE MISLOLA), and the European Community (Project Past4Future).

References

Acker, J. G., and G. Leptoukh (2007), Online analysis enhances use of NASA Earth science data, *Eos Trans. AGU*, *88*(2), 14, doi:10.1029/2007EO020003.

Algeo, T. J., and J. B. Maynard (2004), Trace-element behavior and redox facies in core shales of Upper Pennsylvanian Kansas-type cyclothems, *Chem. Geol.*, *206*(3–4), 289–318, doi:10.1016/j.chemgeo.2003.12.009.

Altabet, M. A., M. J. Higginson, and D. W. Murray (2002), The effect of millennial-scale changes in Arabian Sea denitrification on atmospheric CO_2, *Nature*, *415*(6868), 159–162, doi:10.1038/415159a.

Asmerom, Y., V. J. Polyak, and S. J. Burns (2010), Variable winter moisture in the southwestern United States linked to rapid glacial climate shifts, *Nat. Geosci.*, *3*(2), 114–117, doi:10.1038/ngeo754.

Beaufort, L., et al. (2002), MD126-IMAGES VIII Marges Ouest Nord Américaines (MONA), cruise report, Inst. Paul Emile Victor, Plouzané, France.

Benson, L., S. Lund, R. Negrini, B. Linsley, and M. Zic (2003), Response of North American Great Basin Lakes to Dansgaard-Oeschger oscillations, *Quat. Sci. Rev.*, *22*(21–22), 2239–2251, doi:10.1016/S0277-3791(03)00210-5.

Blanchet, C. L., N. Thouveny, and T. de Garidel-Thoron (2006), Evidence for multiple paleomagnetic intensity lows between 30 and 50 ka BP from a western Equatorial Pacific sedimentary sequence, *Quat. Sci. Rev.*, *25*(9–10), 1039–1052, doi:10.1016/j.quascirev.2005.09.001.

Blanchet, C. L., N. Thouveny, L. Vidal, G. Leduc, K. Tachikawa, E. Bard, and L. Beaufort (2007), Terrigenous input response to glacial/interglacial climatic variations over southern Baja California: A rock magnetic approach, *Quat. Sci. Rev.*, *26*(25–28), 3118–3133, doi:10.1016/j.quascirev.2007.07.008.

Böning, P., H.-J. Brumsack, M. E. Böttcher, B. Schnetger, C. Kriete, J. Kallmeyer, and S. L. Borchers (2004), Geochemistry of Peruvian near-surface sediments, *Geochim. Cosmochim. Acta*, *68*(21), 4429–4451, doi:10.1016/j.gca.2004.04.027.

Bostock, H. C., B. N. Opdyke, and M. J. M. Williams (2010), Characterising the intermediate depth waters of the Pacific Ocean using $\delta^{13}C$ and other geochemical tracers, *Deep Sea Res., Part I*, *57*(7), 847–859, doi:10.1016/j.dsr.2010.04.005.

Boyle, E. A., F. R. Sclater, and J. M. Edmond (1977), The distribution of dissolved copper in the Pacific, *Earth Planet. Sci. Lett.*, *37*(1), 38–54, doi:10.1016/0012-821X(77)90144-3.

Broecker, W., G. Bond, M. Klas, E. Clark, and J. McManus (1992), Origin of the northern Atlantic's Heinrich events, *Clim. Dyn.*, *6*(3–4), 265–273.

Calvert, S. E., and T. F. Pedersen (1993), Geochemistry of recent oxic and anoxic marine sediments: Implications for the geological record, *Mar. Geol.*, *113*(1–2), 67–88, doi:10.1016/0025-3227(93)90150-T.

Calvert, S. E., and T. F. Pedersen (1996), Sedimentary geochemistry of manganese: Implications for the environment of formation of manganiferous black shales, *Econ. Geol.*, *91*(1), 36–47, doi:10.2113/gsecongeo.91.1.36.

Calvert, S. E., and T. F. Pedersen (2007), Chapter fourteen elemental proxies for palaeoclimatic and palaeoceanographic variability in marine sediments: Interpretation and application, in *Developments in Marine Geology: Proxies in Late Cenozoic Paleoceanography*, edited by C. Hillaire-Marcel and A. De Vernal, pp. 567–644, Elsevier, Amsterdam.

Cannariato, K. G., and J. P. Kennett (1999), Climatically related millennial-scale fluctuations in strength of California margin oxygen-minimum zone during the past 60 k.y., *Geology*, *27*(11), 975–978, doi:10.1130/0091-7613(1999)027<0975:CRMSFI>2.3.CO;2.

Clement, A. C., and L. C. Peterson (2008), Mechanisms of abrupt climate change of the last glacial period, *Rev. Geophys.*, *46*, RG4002, doi:10.1029/2006RG000204.

Croudace, I. W., A. Rindby, and R. G. Rothwell (2006), ITRAX: Description and evaluation of a new multi-function X-ray core scanner, in *New Techniques in Sediment Core Analysis*, *Geol. Soc. Spec. Publ.*, 267, 51–63.

Curry, W. B., and D. W. Oppo (2005), Glacial water mass geometry and the distribution of $\delta^{13}C$ of ΣCO_2 in the western Atlantic Ocean, *Paleoceanography*, *20*, PA1017, doi:10.1029/2004PA001021.

Dansgaard, W., et al. (1993), Evidence for general instability of past climate from 250-kyr ice-core record, *Nature*, *364*(6434), 218–220, doi:10.1038/364218a0.

Dean, W. E. (2007), Sediment geochemical records of productivity and oxygen depletion along the margin of western North America during the past 60,000 years: Teleconnections with Greenland Ice and the Cariaco Basin, *Quat. Sci. Rev.*, *26*(1–2), 98–114, doi:10.1016/j.quascirev.2006.08.006.

Dean, W. E., J. V. Gardner, and D. Z. Piper (1997), Inorganic geochemical indicators of glacial-interglacial changes in productivity and anoxia on the California continental margin, *Geochim. Cosmochim. Acta*, *61*(21), 4507–4518, doi:10.1016/S0016-7037(97)00237-8.

Dean, W. E., Y. Zheng, J. D. Ortiz, and A. van Geen (2006), Sediment Cd and Mo accumulation in the oxygen-minimum zone off western Baja California linked to global climate over the past 52 kyr, *Paleoceanography*, *21*, PA4209, doi:10.1029/2005PA001239.

Dittert, N., and R. Henrich (2000), Carbonate dissolution in the South Atlantic Ocean: Evidence from ultrastructure breakdown in Globigerina bulloides, *Deep Sea Res., Part I*, *47*(4), 603–620, doi:10.1016/S0967-0637(99)00069-2.

Durazo, R., and T. R. Baumgartner (2002), Evolution of oceanographic conditions off Baja California: 1997–1999, *Prog. Oceanogr.*, *54*(1–4), 7–31, doi:10.1016/S0079-6611(02)00041-1.

Galbraith, E. D., M. Kienast, T. F. Pedersen, and S. E. Calvert (2004), Glacial-interglacial modulation of the marine nitrogen cycle by high-latitude O_2 supply to the global thermocline, *Paleoceanography*, *19*, PA4007, doi:10.1029/2003PA001000.

Ganeshram, R. S., and T. F. Pedersen (1998), Glacial-interglacial variability in upwelling and bioproductivity off NW Mexico: Implications for quaternary paleoclimate, *Paleoceanography*, *13*(6), 634–645, doi:10.1029/98PA02508.

Ganeshram, R. S., T. F. Pedersen, S. E. Calvert, G. W. McNeill, and M. R. Fontugne (2000), Glacial-interglacial variability in denitrification in the world's oceans: Causes and consequences, *Paleoceanography*, *15*(4), 361–376, doi:10.1029/1999PA000422.

Gay, P. S., and T. K. Chereskin (2009), Mean structure and seasonal variability of the poleward undercurrent off southern California, *J. Geophys. Res.*, *114*, C02007, doi:10.1029/2008JC004886.

Giraud, X., and A. Paul (2010), Interpretation of the paleo-primary production record in the NW African coastal upwelling system as potentially biased by sea level change, *Paleoceanography*, *25*, PA4224, doi:10.1029/2009PA001795.

Guidi, L., G. Gorsky, H. Claustre, M. Picheral, and L. Stemmann (2008), Contrasting distribution of aggregates >100 μm in the upper kilometre of the south-eastern Pacific, *Biogeosciences Discuss.*, *5*(1), 871–901, doi:10.5194/bgd-5-871-2008.

Harada, N., N. Ahagon, T. Sakamoto, M. Uchida, M. Ikehara, and Y. Shibata (2006), Rapid fluctuation of alkenone temperature in the southwestern Okhotsk Sea during the past 120 ky, *Global Planet. Change*, *53*(1–2), 29–46, doi:10.1016/j.gloplacha.2006.01.010.

Heinrich, H. (1988), Origin and consequences of cyclic ice rafting in the Northeast Atlantic Ocean during the past 130,000 years, *Quat. Res.*, *29*(2), 142–152, doi:10.1016/0033-5894(88)90057-9.

Hendy, I. L., and J. P. Kennett (2003), Tropical forcing of North Pacific intermediate water distribution during Late Quaternary rapid climate change?, *Quat. Sci. Rev.*, *22*(5–7), 673–689, doi:10.1016/S0277-3791(02)00186-5.

Hendy, I. L., and T. F. Pedersen (2005), Is pore water oxygen content decoupled from productivity on the California Margin? Trace element results from Ocean Drilling Program Hole 1017E, San Lucia slope, California, *Paleoceanography*, *20*, PA4026, doi:10.1029/2004PA001123.

Hendy, I. L., and T. F. Pedersen (2006), Oxygen minimum zone expansion in the eastern tropical North Pacific during deglaciation, *Geophys. Res. Lett.*, *33*, L20602, doi:10.1029/2006GL025975.

Hendy, I. L., J. P. Kennett, E. B. Roark, and B. L. Ingram (2002), Apparent synchroneity of submillennial scale climate events between Greenland and Santa Barbara Basin, California from 30–10 ka, *Quat. Sci. Rev.*, *21*(10), 1167–1184, doi:10.1016/S0277-3791(01)00138-X.

Hendy, I. L., T. F. Pedersen, J. P. Kennett, and R. Tada (2004), Intermittent existence of a southern Californian upwelling cell during submillennial climate change of the last 60 kyr, *Paleoceanography*, *19*, PA3007, doi:10.1029/2003PA000965.

Herguera, J. C., T. Herbert, M. Kashgarian, and C. Charles (2010), Intermediate and deep water mass distribution in the Pacific during the Last Glacial Maximum inferred from oxygen and carbon stable isotopes, *Quat. Sci. Rev.*, *29*(9–10), 1228–1245 doi:10.1016/j.quascirev.2010.02.009.

Hickey, B. M. (1998), Coastal oceanography of western North America from the tip of Baja California to Vancouver Island, *The Sea*, *11*, 345–393.

Ivanochko, T. S., and T. F. Pedersen (2004), Determining the influences of Late Quaternary ventilation and productivity variations on Santa Barbara Basin sedimentary oxygenation: A multi-proxy approach, *Quat. Sci. Rev.*, *23*(3–4), 467–480, doi:10.1016/j.quascirev.2003.06.006.

Johnsen, S. J., D. Dahl-Jensen, N. Gundestrup, J. P. Steffensen, H. B. Clausen, H. Miller, V. Masson-Delmotte, A. E. Sveinbjörnsdottir, and J. White (2001), Oxygen isotope and palaeotemperature records from six Greenland ice-core stations: Camp Century, Dye-3, GRIP, GISP2, Renland and NorthGRIP, *J. Quaternary Sci.*, *16*(4), 299–307, doi:10.1002/jqs.622.

Keigwin, L. D. (1998), Glacial-age hydrography of the far northwest Pacific Ocean, *Paleoceanography*, *13*(4), 323–339, doi:10.1029/98PA00874.

Kienast, S. S., S. E. Calvert, and T. F. Pedersen (2002), Nitrogen isotope and productivity variations along the northeast Pacific margin over the last 120 kyr: Surface and subsurface paleoceanography, *Paleoceanography*, *17*(4), 1055, doi:10.1029/2001PA000650.

Klinkhammer, G. P., and M. R. Palmer (1991), Uranium in the oceans: Where it goes and why, *Geochim. Cosmochim. Acta*, *55*(7), 1799–1806, doi:10.1016/0016-7037(91)90024-Y.

Kutzbach, J. E., and H. E. Wright Jr. (1985), Simulation of the climate of 18,000 years BP: Results for the North American/North Atlantic/European sector and comparison with the geologic record of North America, *Quat. Sci. Rev.*, *4*(3), 147–187, doi:10.1016/0277-3791(85)90024-1.

Ladah, L. B. (2003), The shoaling of nutrient-enriched subsurface waters as a mechanism to sustain primary productivity off central Baja California during El Niño winters, *J. Mar. Syst.*, *42*(3–4), 145–152, doi:10.1016/S0924-7963(03)00072-1.

Leduc, G., L. Vidal, K. Tachikawa, F. Rostek, C. Sonzogni, L. Beaufort, and E. Bard (2007), Moisture transport across Central America as a positive feedback on abrupt climatic changes, *Nature*, *445*(7130), 908–911, doi:10.1038/nature05578.

Marchal, O., T. F. Stocker, and F. Joos (1998), Impact of oceanic reorganizations on the ocean carbon cycle and atmospheric carbon dioxide content, *Paleoceanography*, *13*(3), 225–244, doi:10.1029/98PA00726.

Marchitto, T. M., S. J. Lehman, J. D. Ortiz, J. Fluckiger, and A. van Geen (2007), Marine radiocarbon evidence for the mechanism of deglacial atmospheric CO_2 rise, *Science*, *316*(5830), 1456–1459, doi:10.1126/science.1138679.

Matsumoto, K., T. Oba, J. Lynch-Stieglitz, and H. Yamamoto (2002), Interior hydrography and circulation of the glacial Pacific Ocean, *Quat. Sci. Rev.*, *21*(14–15), 1693–1704, doi:10.1016/S0277-3791(01)00142-1.

Mayer, L. M., L. L. Schick, M. A. Allison, K. C. Ruttenberg, and S. J. Bentley (2007), Marine vs. terrigenous organic matter in Louisiana coastal sediments: The uses of bromine: organic carbon ratios, *Mar. Chem.*, *107*(2), 244–254, doi:10.1016/j.marchem.2007.07.007.

McCartney, M. S. (1977), Water mass renewal in sub-Antarctic zone, *Antarct. J. US.*, *12*(4), 54–56.

McLennan, S. M. (2001), Relationships between the trace element composition of sedimentary rocks and upper continental crust, *Geochem. Geophys. Geosyst.*, *2*(4), 1021, doi:10.1029/2000GC000109.

McManus, J. F., R. Francois, J. M. Gherardi, L. D. Keigwin, and S. Brown-Leger (2004), Collapse and rapid resumption of Atlantic meridional circulation linked to deglacial climate changes, *Nature*, *428*, 834–837, doi:10.1038/nature02494.

Mikolajewicz, U., T. J. Crowley, A. Schiller, and R. Voss (1997), Modelling teleconnections between the North Atlantic and North Pacific during the Younger Dryas, *Nature*, *387*(6631), 384–387, doi:10.1038/387384a0.

Muratli, J. M., Z. Chase, A. C. Mix, and J. McManus (2010), Increased glacial-age ventilation of the Chilean margin by Antarctic Intermediate Water, *Nat. Geosci.*, *3*(1), 23–26, doi:10.1038/ngeo715.

Murdmaa, I. O., G. H. Kazarina, L. Beaufort, E. V. Ivanova, E. M. Emelyanov, V. A. Kravtsov, G. N. Alekhina, and V. E. Vasileva (2010), Upper quaternary laminated sapropelic sediments from the continental slope of Baja California, *Lithology Mineral Resour.*, *45*, 154–171.

Nameroff, T. J., L. S. Balistrieri, and J. W. Murray (2002), Suboxic trace metal geochemistry in the eastern tropical North Pacific, *Geochim. Cosmochim. Acta*, *66*(7), 1139–1158, doi:10.1016/S0016-7037(01)00843-2.

Nameroff, T. J., S. E. Calvert, and J. W. Murray (2004), Glacial-interglacial variability in the eastern tropical North Pacific oxygen minimum zone recorded by redox-sensitive trace metals, *Paleoceanography*, *19*, PA1010, doi:10.1029/2003PA000912.

Nederbragt, A. J., J. W. Thurow, and P. R. Bown (2008), Paleoproductivity, ventilation, and organic carbon burial in the Santa Barbara Basin (ODP Site 893, off California) since the last glacial, *Paleoceanography*, *23*, PA1211, doi:10.1029/2007PA001501.

Okazaki, Y., A. Timmermann, L. Menviel, N. Harada, A. Abe-Ouchi, M. O. Chikamoto, A. Mouchet, and H. Asahi (2010), Deepwater formation in the North Pacific during the Last Glacial Termination, *Science*, *329*(5988), 200–204, doi:10.1126/science.1190612.

Okumura, Y. M., C. Deser, A. Hu, A. Timmermann, and S. P. Xie (2009), North Pacific climate response to freshwater forcing in the subarctic North Atlantic: Oceanic and atmospheric pathways, *J. Clim.*, *22*(6), 1424–1445, doi:10.1175/2008JCLI2511.1.

Ortiz, J. D., S. B. O'Connell, J. DelViscio, W. Dean, J. D. Carriquiry, T. Marchitto, Y. Zheng, and A. van Geen (2004), Enhanced marine productivity off western North America during warm climate intervals of the past 52 ky, *Geology*, *32*(6), 521–524, doi:10.1130/G20234.1.

Paillard, D., L. Labeyrie, and P. Yiou (1996), Macintosh program performs time-series analysis, *Eos Trans. AGU*, *77*(39), 379, doi:10.1029/96EO00259.

Pailler, D., and E. Bard (2002), High frequency palaeoceanographic changes during the past 140,000 yr recorded by the organic matter in sediments of the Iberian Margin, *Palaeogeogr. Palaeoclimatol. Palaeoecol.*, *181*(4), 431–452, doi:10.1016/S0031-0182(01)00444-8.

Pailler, D., E. Bard, F. Rostek, Y. Zheng, R. Mortlock, and A. van Geen (2002), Burial of redox-sensitive metals and organic matter in the equatorial Indian Ocean linked to precession, *Geochim. Cosmochim. Acta*, *66*(5), 849–865, doi:10.1016/S0016-7037(01)00817-1.

Paulmier, A., and D. Ruiz-Pino (2009), Oxygen minimum zones (OMZs) in the modern ocean, *Prog. Oceanogr.*, *80*(3–4), 113–128, doi:10.1016/j.pocean.2008.08.001.

Pérez-Brunius, P., M. López, and J. Pineda (2006), Hydrographic conditions near the coast of northwestern Baja California: 1997–2004, *Cont. Shelf Res.*, *26*(8), 885–901, doi:10.1016/j.csr.2006.01.017.

Pichevin, L. E., R. S. Ganeshram, S. Francavilla, E. Arellano-Torres, T. F. Pedersen, and L. Beaufort (2010), Interhemispheric leakage of isotopically heavy nitrate in the eastern tropical Pacific during the last glacial period, *Paleoceanography*, *25*, PA1204, doi:10.1029/2009PA001754.

Pierce, S. D., R. L. Smith, P. M. Kosro, J. A. Barth, and C. D. Wilson (2000), Continuity of the poleward undercurrent along the eastern boundary of the mid-latitude North Pacific, *Deep Sea Res., Part II*, *47*(5–6), 811–829, doi:10.1016/S0967-0645(99)00128-9.

Romanova, V., G. Lohmann, K. Grosfeld, and M. Butzin (2006), The relative role of oceanic heat transport and orography on glacial climate, *Quat. Sci. Rev.*, *25*(7–8), 832–845, doi:10.1016/j.quascirev.2005.07.007.

Saenko, O. A., A. Schmittner, and A. J. Weaver (2004), The Atlantic-Pacific seesaw, *J. Clim.*, *17*(11), 2033–2038, doi:10.1175/1520-0442(2004)017<2033:TAS>2.0.CO;2.

Schenau, S. J., M. A. Prins, G. J. De Lange, and C. Monnin (2001), Barium accumulation in the Arabian Sea: Controls on barite preservation in marine sediments, *Geochim. Cosmochim. Acta*, *65*(10), 1545–1556, doi:10.1016/S0016-7037(01)00547-6.

Schmittner, A., E. D. Galbraith, S. W. Hostetler, T. F. Pedersen, and R. Zhang (2007), Large fluctuations of dissolved oxygen in the Indian and Pacific oceans during Dansgaard-Oeschger oscillations caused by variations of North Atlantic Deep Water subduction, *Paleoceanography*, *22*, PA3207, doi:10.1029/2006PA001384.

Schulte, S., F. Rostek, E. Bard, J. Rullkotter, and O. Marchal (1999), Variations of oxygen-minimum and primary productivity recorded in sediments of the Arabian Sea, *Earth Planet. Sci. Lett.*, *173*(3), 205–221, doi:10.1016/S0012-821X(99)00232-0.

Schulz, H., U. von Rad, and H. Erlenkeuser (1998), Correlation between Arabian Sea and Greenland climate oscillations of the past 110,000 years, *Nature*, *393*(6680), 54–57.

Shcherbina, A. Y., L. D. Talley, and D. L. Rudnick (2003), Direct observations of North Pacific ventilation: Brine rejection in the Okhotsk Sea, *Science*, *302*(5652), 1952–1955, doi:10.1126/science.1088692.

Shimmield, G. B., and N. B. Price (1986), The behaviour of molybdenum and manganese during early sediment diagenesis—offshore Baja California, Mexico, *Mar. Chem.*, *19*(3), 261–280, doi:10.1016/0304-4203(86)90027-7.

Takahashi, K. (1998), The Bering and Okhotsk Seas: Modern and past paleoceanographic changes and gateway impact, *J. Asian Earth Sci.*, *16*(1), 49–58, doi:10.1016/S0743-9547(97)00048-2.

Talley, L. D. (1991), An Okhotsk sea-water anomaly Implication for ventilation in the North Pacific, *Deep Sea Res., Part I*, 38, S171–S190.

Thomas, A. C., M. E. Carr, and P. T. Strub (2001), Chlorophyll variability in eastern boundary currents, *Geophys. Res. Lett.*, *28*(18), 3421–3424, doi:10.1029/2001GL013368.

Timmermann, A., U. Krebs, F. Justino, H. Goosse, and T. Ivanochko (2005), Mechanisms for millennial-scale global synchronization during the last glacial period, *Paleoceanography*, *20*, PA4008, doi:10.1029/2004PA001090.

Tjallingii, R., U. Rohl, M. Kolling, and T. Bickert (2007), Influence of the water content on X-ray fluorescence core-scanning measurements in soft marine sediments, *Geochem. Geophys. Geosyst.*, *8*, Q02004, doi:10.1029/2006GC001393.

Tomczak, M., and J. S. Godfrey (Eds.) (2003), *Regional Oceanography: An Introduction*, Pergamon, Oxford, U. K.

Tribovillard, N., T. J. Algeo, T. Lyons, and A. Riboulleau (2006), Trace metals as paleoredox and paleoproductivity proxies: An update, *Chem. Geol.*, *232*(1–2), 12–32, doi:10.1016/j.chemgeo.2006.02.012.

van Geen, A., and D. M. Husby (1996), Cadmium in the California Current system: Tracer of past and present upwelling, *J. Geophys. Res.*, *101*(C2), 3489–3507, doi:10.1029/95JC03302.

van Geen, A., R. G. Fairbanks, P. Dartnell, M. McGann, J. V. Gardner, and M. Kashgarian (1996), Ventilation changes in the northeast Pacific during the last deglaciation, *Paleoceanography*, *11*(5), 519–528, doi:10.1029/96PA01860.

van Geen, A., Y. Zheng, J. M. Bernhard, K. G. Cannariato, J. Carriquiry, W. E. Dean, B. W. Eakins, J. D. Ortiz, and J. Pike (2003), On the preservation of laminated sediments along the western margin of North America, *Paleoceanography*, *18*(4), 1098, doi:10.1029/2003PA000911.

van Geen, A., W. M. Smethie Jr., A. Horneman, and H. Lee (2006), Sensitivity of the North Pacific oxygen minimum zone to changes in ocean circulation: A simple model calibrated by chlorofluorocarbons, *J. Geophys. Res.*, *111*, C10004, doi:10.1029/2005JC003192.

Voss, M., J. W. Dippner, and J. P. Montoya (2001), Nitrogen isotope patterns in the oxygen-deficient waters of the eastern tropical North Pacific Ocean, *Deep Sea Res., Part I*, *48*(8), 1905–1921, doi:10.1016/S0967-0637(00)00110-2.

Waelbroeck, C., L. Labeyrie, E. Michel, J. C. Duplessy, J. F. McManus, K. Lambeck, E. Balbon, and M. Labracherie (2002), Sea-level and deep water temperature changes derived from benthic foraminifera isotopic records, *Quat. Sci. Rev.*, *21*(1–3), 295–305, doi:10.1016/S0277-3791(01)00101-9.

Wagner, J. D. M., J. E. Cole, J. W. Beck, P. J. Patchett, G. M. Henderson, and H. R. Barnett (2010), Moisture variability in the southwestern United States linked to abrupt glacial climate change, *Nat. Geosci.*, *3*(2), 110–113, doi:10.1038/ngeo707.

Zaytsev, O., R. Cervantes-Duarte, O. Montante, and A. Gallegos-Garcia (2003), Coastal upwelling activity on the pacific shelf of the Baja California Peninsula, *J. Oceanogr.*, *59*(4), 489–502, doi:10.1023/A:1025544700632.

Zheng, Y., A. van Geen, R. F. Anderson, J. V. Gardner, and W. E. Dean (2000), Intensification of the northeast Pacific oxygen minimum zone during the Bolling-Allerod warm period, *Paleoceanography*, *15*(5), 528–536, doi:10.1029/1999PA000473.

Ziegler, M., T. Jilbert, G. J. de Lange, L. J. Lourens, and G. J. Reichart (2008), Bromine counts from XRF scanning as an estimate of the marine organic carbon content of sediment cores, *Geochem. Geophys. Geosyst.*, *9*, Q05009, doi:10.1029/2007GC001932.

E. Bard, O. Cartapanis, and K. Tachikawa, CEREGE, Aix-Marseille Université, CNRS, IRD, College de France, Technopole de l'Arbois, BP 80, F-13545 Aix en Provence, France. (cartapanis@cerege.fr)